UNIVERSIDADE ESTADUAL DE MARINGÁ
PÓS GRADUAÇÃO EM FÍSICA

Gabriel Antonio Flizikowski Siqueira

INVESTIGAÇÃO DAS PROPRIEDADES ESPECTROSCÓPICAS E TEORIA DE JUDD-OFELT EM VIDROS ALUMINOSILICATOS DE CÁLCIO DOPADOS COM PRASEODÍMIO

Orientador: **Prof. Dr. Luis Carlos Malacarne**
Co-orientador: **Prof. Dr. Nelson Guilherme Castelli Astrath**

Maringá, Março de 2018

UNIVERSIDADE ESTADUAL DE MARINGÁ
PÓS GRADUAÇÃO EM FÍSICA

Gabriel Antonio Flizikowski Siqueira

INVESTIGATION ON THE SPECTROSCOPIC PROPERTIES AND JUDD-OFELT THEORY IN CALCIUM ALUMINOSILICATE GLASSES DOPED WITH PRASEODYMIUM

Supervisor: **Prof. Dr. Luis Carlos Malacarne**
Co-supervisor: **Prof. Dr. Nelson Guilherme Castelli Astrath**

Maringá, March 2018

UNIVERSIDADE ESTADUAL DE MARINGÁ
PÓS GRADUAÇÃO EM FÍSICA

Gabriel Antonio Flizikowski Siqueira

INVESTIGAÇÃO DAS PROPRIEDADES ESPECTROSCÓPICAS E TEORIA DE JUDD-OFELT EM VIDROS ALUMINOSILICATOS DE CÁLCIO DOPADOS COM PRASEODÍMIO

Dissertação de Mestrado apresentada ao Departamento de Física da Universidade Estadual de Maringá para a obtenção do título de Mestre em Física.

Banca Examinadora:

Prof. Dr. Luis Carlos Malacarne - UEM (Orientador)
Prof. Dr. Tomaz Catunda - USP - São Carlos
Prof. Dr. Luiz Fernando Cótica - UEM
Prof. Dr. Tomaž Požar - University of Ljubljana (Suplente)
Prof. Dr. Nelson Guilherme Castelli Astrath - UEM (Coorientador)(Suplente)

Maringá, Março de 2018

UNIVERSIDADE ESTADUAL DE MARINGÁ
PÓS GRADUAÇÃO EM FÍSICA

Gabriel Antonio Flizikowski Siqueira

INVESTIGATION ON THE SPECTROSCOPIC PROPERTIES AND JUDD-OFELT THEORY IN CALCIUM ALUMINOSILICATE GLASSES DOPED WITH PRASEODYMIUM

Master's Dissertation presented to the Departamento de Física of the Universidade Estadual de Maringá to obtain the Master's Degree in Physics.

Supervisory Commitee:

Prof. Dr. Luis Carlos Malacarne - UEM (Supervisor)
Prof. Dr. Tomaz Catunda - USP - São Carlos
Prof. Dr. Luiz Fernando Cótica - UEM
Prof. Dr. Tomaž Požar - University of Ljubljana (Alternate)
Prof. Dr. Nelson Guilherme Castelli Astrath - UEM (Co-supervisor)(Alternate)

Maringá, March 2018

Dados Internacionais de Catalogação na Publicação (CIP)
(Biblioteca Central - UEM, Maringá, PR, Brasil)

Siqueira, Gabriel Antonio Flizikowski
S618i Investigação das propriedades espectroscópicas e teoria de Judd-Ofelt em vidros aluminosilicatos de cálcio dopados com praseodímio. / Gabriel Flizikowiski Siqueira. -- Maringá, 2018.
56 f. : il., color, figs., tabs.

Orientador(a): Prof. Dr. Luis Carlos Malacarne.
Co-orientador(a). Prof. Dr. Nelson Guilherme Castelli Astrath.
Dissertação (mestrado) - Universidade Estadual de Maringá, Centro de Ciências Exatas, Departamento de Física, Programa de Pós-Graduação em Física, 2018.

1. Conversão ascendente. 2. Praseodímio. 3. Hipersensitividade. 4. Aluminosilicato. 5. Decaimento não-exponencial. 6. CAS:Pr^{3+}. 7. LCAS:Pr^{3+}. 8. Teoria de Judd-Ofelt padrão. 9. Teoria de Judd-Ofelt modificada. I. Malacarne, Luis Carlos, orient. II. Astrath, Nelson Guilherme Castelli. III. Universidade Estadual de Maringá. Centro de Ciências Exatas. Departamento de Física. Programa de Pós-Graduação em Física. IV. Título.

CDD 21.ed. 535.35
AHS-crB-9/1065

Contents

List of Figures

List of Tables

À minha mãe, por tudo que enfrentou
para que seus filhos tivessem uma boa educação.

"One, remember to look up at the stars and not down at your feet. Two, never give up work. Work gives you meaning and purpose and life is empty without it. Three, if you are lucky enough to find love, remember it is there and don't throw it away."

Stephen Hawking, 2006

Acknowledgments

Foremost, I would like to express my sincere gratitude to my advisor and co-advisor, Prof. Dr. Luis Carlos Malacarne and Prof. Dr. Nelson Guilherme Castelli Astrath for accepting me, for the support of my Master's study and research, for their patience and knowledge.

I would like to profoundly thank Vitor Santaella Zanuto. His guidance helped me in all the time of research and writing of this thesis.

I thank all my fellow labmates. This work would not be complete if there were no conversations — insightful or not insightful at all — with coffee and good laughs, in the research/writing process.

To my mother, Marilena, who have provided me all moral and emotional support in my life and to all my family because I owe it all to you and I love you.

Thank you immensely to my girlfriend Kim, for all her unconditional love and infinite support.

To my dear friends, thanks for the support!

To all the DFI/PFI collaborators, specially to Monica for the attention and services provided by the secretary.

I acknowledge the support from the Brazilian agencies CAPES, CNPq, Fundação Araucária and FINEP.

Resumo

A teoria de Judd-Ofelt é conhecida por ser menos efetiva quando aplicada em matrizes dopadas com Pr^{3+}, isso geralmente é atribuído à pequena diferença de energia entre o nível fundamental e a primeira configuração de paridade oposta. Algumas teorias modificadas foram desenvolvidas no passado para resolver o problema. Neste estudo, apresentamos uma investigação detalhada sobre dois conjuntos de vidros aluminosilicatos de cálcio, um com 34% de Si_2O (CAS) e outro com 7% de Si_2O (LSCAS), ambos os conjuntos dopados com diferentes concentrações de Pr^{3+} (0,2; 0,5; 1.0 e 2.0 % em massa). Transições ópticas para os níveis $^3H_4 \rightarrow {}^3P_{0,\,1,\,2}$; $^1I_6$; $^1D_2$; $^1G_4$; $^3F_{2,\,3,\,4}$ e $^3H_6$ foram observadas usando espectroscopia UV–VIS–NIR a temperatura ambiente. As emissões dos níveis $^3P_0$ e $^1D_2$ foram detectadas e as curvas se afastam do comportamento exponencial. A conversão ascendente para UV também foi observada quando as amostras foram excitadas no nível ^3P_j, populando o nível superior 4f5d — por conversão ascendente por transferência de energia e/ou absorção de estado excitado — que decai emitindo luz UV. Além disso, a variação incomum das intensidades dos picos das transições $^3P_0 \rightarrow {}^3F_2$ e $^3P_0 \rightarrow {}^3F_4$ sugere que eles são hipersensíveis, embora a transição eletrônica $^3P_0 \rightarrow {}^3F_4$ não obedeça inteiramente à todas as regras de seleção clássicas. A teoria padrão de Judd-Ofelt foi aplicada. Os resultados e quantidades espectroscópicas derivadas — tais como probabilidades de transição, tempos de vida radiativo e razões de ramificação — foram comparados com os de algumas teorias modificadas de Judd-Ofelt. Os resultados mostraram que as teorias modificadas podem levar a valores menores do desvio quadrático médio. No entanto, uma melhor concordância entre os dados experimentais e a teoria padrão foi observada quando as quantidades espectroscópicas derivadas são levadas em consideração. Além disso, os resultados para a razão de ramificação das transições $^3P_0 \rightarrow {}^3H_4$ e $^1D_2 \rightarrow {}^3H_4$ foram de mais de 60% para as duas matrizes de vidro, sugerindo o seu potencial uso como dispositivos laser de estado sólido.

Palavras-chave: conversão ascendente, praseodímio, hipersensitividade, aluminosilicato, decaimento não-exponencial, CAS:Pr^{3+}, LSCAS:Pr^{3+}, teoria de Judd-Ofelt padrão, teoria de Judd-Ofelt modificada.

Abstract

The Judd-Ofelt theory is known to be less effective when applied to Pr^{3+}-doped hosts, this is usually attributed to the small energy difference between the fundamental level and the first opposite parity configuration. Some modified theories have been developed in the past in order to work around the problem. In this study, we present a detailed investigation on two sets of calcium aluminosilicate glasses, one with 34% of Si_2O (CAS) and another with 7% of Si_2O (LSCAS), both sets doped with different concentrations of Pr^{3+} (0.2, 0.5, 1.0 and 2.0 wt.%). Optical transitions for the levels $^3H_4 \rightarrow {}^3P_{0,\,1,\,2}$; $^1I_6$; $^1D_2$; $^1G_4$; $^3F_{2,\,3,\,4}$ and $^3H_6$ have been observed using UV–VIS–NIR spectroscopy at room temperature. Emissions from levels $^3P_0$ and $^1D_2$ were detected and curves deviate from exponential behavior. Upconversion to UV was also observed when samples were excited in the ^3P_j level, populating the 4f5d upper level — via energy transfer upconversion and/or excited state absorption — which decays emitting UV light. In addition, the unusual variation of the peak intensities of transitions $^3P_0 \rightarrow {}^3F_2$ and $^3P_0 \rightarrow {}^3F_4$ suggests they are hypersensitive, although the $^3P_0 \rightarrow {}^3F_4$ electronic transition does not entirely obey all the classic selection rules. The standard Judd-Ofelt theory was applied. The results and derived spectroscopic quantities — such as transition probabilities, radiative lifetimes and branching ratios — were compared to a couple of modified Judd-Ofelt theories. Results showed the modified theories can lead to smaller values of root mean square deviations. However, a better agreement between experimental data and the standard theory has been remarked when the derived spectroscopic quantities are taken into account. Moreover, results for the branching ratio of the $^3P_0 \rightarrow {}^3H_4$ and $^1D_2 \rightarrow {}^3H_4$ transitions were over 60% for both glass hosts, suggesting its potential use as solid-state laser devices.

Keywords: upconversion, praseodymium, hypersensitive, aluminosilicate, non-exponential decay, CAS:Pr^{3+}, LSCAS:Pr^{3+}, standard Judd-Ofelt theory, modified Judd-Ofelt theory

Chapter 1

Introduction

The great potentiality of rare-earth elements as optically active ions in a wide variety of host materials is, up to a certain point, accounted for the minimal influence of the host crystal field, provided by the external electronic shells shielding, in the emissions of the intraconfigurational 4f transitions. In this context, the third ionized state of praseodymium (Pr^{3+}) is highlighted among other rare-earth elements as consequence of its large variety of transitions. Trivalent praseodymium ion has been widely used for doping optical materials due to a broad infrared emission, which makes it interesting for telecommunication applications. Besides the infrared emission, Pr^{3+}–doped glasses exhibit a large visible emission spectrum, which comprises blue, green and orange-red emissions, depending on the host matrices [1]. As red emitting devices, these materials present great potential in medical therapies due to the optical skin transmittance [2]. Alongside the variety of possible emissions, Pr^{3+} can also emit in the UV range when excited in the 4d5f level directly or via upconversion mechanisms.

Pr^{3+} have been studied in many different hosts, such as fluorite [3–5], borate [6–10]; phosphate [11, 12]; tellurite [13, 14] and aluminosilicate glasses [2]. However, Pr^{3+}-doped calcium aluminosilicate glasses were reported only when co-doped with ytterbium (Yb^{3+}) [15], in which the authors investigated the occurrence of energy transfer processes from Pr^{3+} to Yb^{3+}. The interest in these glasses is due to their good thermo-optical and mechanical properties compared to silicates and phosphates [16], elevated transition temperature and transparency up to 5 μm [17, 18]. Investigations have been done concerning the compositional dependence of the physical properties of the calcium aluminosilicate glasses [16, 19]. When doped with rare-earth elements, studies have shown these glasses are potential candidates for optical devices such as tunable white light systems [19, 20] and solid state lasers [19, 21, 22]. For a more detailed work on the structure of rare-earth doped glasses the reader is encouraged to check Refs. [23, 24].

Upconversion processes have been extensively studied for applications such as converting low-energy laser radiation into high-energy radiation by exchanging two or more low energy photons for one high energy photon. This process has increased the response of solar cells in particular wavelengths [25–29], and more recently, studies showed the possibility to diagnose the Ebola virus using upconverting nanoparticles [30]. For Pr^{3+}, upconversion to UV has been studied, for instance, in ceramics [31] and crystals [32–34] and its origin could be due to energy transfer upconversion and/or simultaneous absorption of photons.

Despite the shielding of the 4f–4f transitions that makes rare-earth elements unique, some transitions are quite sensitives to the dopant environment, causing an unconventional alteration in the emission intensity. These are called hypersensitive transitions, and reports showed they are affected by the dopant coordination, site symmetry, and ligand covalency [35, 36]. These transitions, specifically, can be used in optical fiber amplifiers and lasers [35].

The luminescent properties of trivalent rare-earth elements have been described with reasonable success by the Judd-Ofelt (J–O) theory [37, 38]. However, describing the optical spectrum of Pr^{3+} certain issues emerge, usually attributed to the low energy difference between the fundamental level and the first opposite parity excited configuration, $4f^2$ and 4f5d, respectively. Consequences include relatively large values of the root mean square, which measures the agreement between experimental and calculated line strengths, and eventual negative values for the phenomenological Judd-Ofelt parameters Ω_k, which are not consistent with the theoretical definition [39]. These issues, specially concerning the Pr^{3+}, demonstrate there are some aspects in theory of the 4f-4f transitions that are not completely understood yet, thus, additional investigations are necessary.

Objectives

In essence, the present study investigates the spectroscopic properties of calcium aluminosilicate glasses with two different compositions: CAS and low silica CAS (LSCAS) glasses with 34 and 7 wt.% of SiO_2 concentration, respectively. Both compositions with different concentrations of Pr^{3+} as dopant. The optical absorption spectra were obtained for the UV–VIS–NIR range just as the photoluminescence spectra for the UV–VIS–NIR range. Luminescence decay measurements were also carried out to understand the energy processes involving Pr^{3+} ions in this particular glass. The Judd-Ofelt parameters were calculated using the standard and a couple of modified theories in order to get a better insight of the effectiveness of these alternative theories applied to Pr^{3+}-doped calcium aluminosilicate glasses. Moreover, radiative transition probabilities, radiative lifetime and branching ratios were calculated and compared with experimental data.

Chapter 2

Judd-Ofelt theory

The Judd–Ofelt theory (J–O) describes the optical intensities of the 4f-4f transitions of rare-earth elements. The theory was independently developed by Judd [37] and Ofelt [38], in 1962. Essentially, they demonstrated the electric dipole transitions between states are allowed when the rare-earth element is in a medium. The reason of this behavior is the admixing of the first opposite parity configuration $4f^{N-1}5d$ and the fundamental level $4f^{N}$ [9].

Experimental line strength S_{exp} represents the intensity of the absorption band of a transition, which is obtained from the absorption spectrum as follows[1] [9,23,40]

$$S_{exp} = \frac{3hc}{8\pi^3 e^2 \chi}\frac{(2J+1)}{\lambda N}\int \alpha(\lambda_m) d\lambda, \tag{2.1}$$

where h is the Planck's constant, c is the speed of light in vacuum, e is the elementary electric charge, $\chi = (n^2+2)^2/9n$ is the Lorentz local field correction, in which n is the medium refractive index. Total angular momentum of the ground state is represented by J, λ_m is the mean wavelength of the absorption band in nm, N is the number of Pr^{3+} per unit of volume in ions/cm^3 and $\alpha(\lambda)$ the absorption coefficient as a function of the wavelength.

2.0.1 Standard theory

Since the magnetic dipole component for Pr^{3+} can the neglected [12], the calculated line strength according to standard J–O theory is given by the electric dipole

---

[1] Since the J–O theory is widely studied and there are many texts describing the theoretical development, the present text presents a brief description of the main used theoretical parameters, focusing in the application of the theory in the experimental results.

line strength,

$$\mathrm{S_{cal}} = \sum_{k=2,4,6} \Omega_k \left| \langle 4fSLJ|\, U^{(k)}\, |4fS'L'J'\rangle \right|^2, \tag{2.2}$$

where Ω_k is the intensity parameter of rank k, or the so called J–O parameters, and $\left| \langle 4fSLJ|\, U^{(k)}\, |4fS'L'J'\rangle \right|^2$ is the squared reduced matrix elements of the unit tensor[2] $U^{(k)}$. The intensity parameters can be evaluated minimizing the difference between the experimental line strengths (Eq. 2.1) of certain amount of absorption bands, and the calculated line strengths (Eq. 2.2), usually by least squares method. The quality of results are determined by the root mean square deviation between experimental and calculated line strengths using the definition [41],

$$\delta_{\mathrm{rms}} = \sqrt{\sum_i \frac{\left(S^i_{\mathrm{exp}} - S^i_{\mathrm{cal}}\right)^2}{N_{\mathrm{t}} - N_{\mathrm{p}}}}, \tag{2.3}$$

where N_{t} and N_{p} are the number of transitions and the number of parameters, respectively. The sum goes through all transitions. Low values of root mean square deviation denote high quality of J–O parameter values.

The intensity parameters allow to determine some spectroscopic properties. For instance, the radiative emission probabilities from an excited state level J' to a lower state J is given by [9, 23]

$$A_{J'J} = \frac{64\pi^4 e^2 \nu^3 \chi_{\mathrm{emi}}}{3h(2J'+1)} S_{\mathrm{cal}}, \tag{2.4}$$

where $\chi_{\mathrm{emi}} = n(n^2+2)^2/9$ is the local field correction and ν the transition energy in cm^{-1}.

The radiative lifetime of an excited level is related to the sum of all possible decays from that level and is defined as

$$\tau = \frac{1}{\sum_{J'} A_{J',J}}. \tag{2.5}$$

The branching ratio is given by

$$\beta_{J'J} = \frac{A_{J',J}}{\sum_{J'} A_{J',J}}. \tag{2.6}$$

---

[2] The reduced matrix elements for Pr^{3+} were kindly provided by Prof. Dr. Ancizar Flórez Londoño by private communication.

2.0.2 Modified theories

In the case of Pr^{3+}, the energy of 4f5d configuration, which is approximately 50×10^3 cm^{-1}, is very close to some 4f states when compared to other rare-earth elements. Therefore, the energy difference between the 4f5d and 4f states, assumed to be constant in the standard theory, does not seem to be suitable for Pr^{3+} [42]. Hence, the approximation used to derive Eq. 2.2 is unreliable and could lead negative intensity parameters [3,4,6,11,12,43], which has no physical meaning. Consequently, a modified theory must be considered.

Some alternative approaches have been developed in the past. In this work, we compare the results of the standard J–O theory with the method of Kornienko *et al.* [44,45] and Flórez *et al.* [46,47]. Third order perturbation theory was employed by Kornienko *et al.* and they obtained the following expression for the calculated line strength [44,45]

$$\begin{aligned} \mathrm{S_{cal}} &= \sum_{k=2,4,6} \Omega_k[1 + 2\mathcal{A}(E_J + E_{J'} - 2E_{4f})] \\ &\times \left|\langle 4fSLJ|\, U^{(k)}\, |4fS'L'J'\rangle\right|^2, \end{aligned} \tag{2.7}$$

wherein $\mathcal{A} = 1/2E_{4f5d}$, E_{4f5d} is the energy of the 4f5d configuration, which for Pr^{3+} is approximately 50×10^3 cm^{-1}. $E_{J'}$, E_J and E_{4f} are the energies of the upper, lower states and barycenter of the 4f configuration, respectively. Thus, the parameter $\mathcal{A}$ is expected to be $\sim 10^{-5}$ cm for Pr^{3+}, although, it has been often used as a fitting parameter [12,42].

Additional odd rank operators have been considered by Flórez *et al.* and the calculated line strength is written as [46]

$$\begin{aligned} \mathrm{S_{cal}} &= \sum_{k=2,4,6} \Omega_k\left|\langle 4fSLJ|\, U^{(k)}\, |4fS'L'J'\rangle\right|^2 \\ &+ \sum_{k=1,3,5} \xi^2\Omega_k\left|\langle 4fSLJ|\, U^{(k)}\, |4fS'L'J'\rangle\right|^2, \end{aligned} \tag{2.8}$$

where $\xi = \nu/\Delta E$ and ΔE refers to the energy difference between ground state and the first opposite parity excited configuration.

Regardless the modified theory, spectroscopic properties remain the same only with a different S_{cal} in the expression for the transition probability.

Chapter 3

Materials and methods

3.1 Glass synthesis

The glasses were prepared[1] using a vacuum furnace and the precursor oxides were weighed using a digital balance.

Two sets of Pr^{3+}–doped calcium aluminosilicate glass samples were synthesized accordingly to the procedure described in Refs. [21, 22] with over 99.99% of purity reagents. One set with a composition (in wt.%) of 34CaO + (27.9 − x/2)Al_2O_3 + (34 − x/2)SiO_2 + 4.1MgO + xPr_6O_{11}, referenced as CAS:xPr^{3+}, and other composed of (47.4 − x/2)CaO + (41.5 − x/2)Al_2O_3 + 7SiO_2 + 4.1MgO + xPr_6O_{11}, referenced as LSCAS:xPr^{3+}, where x = 0.2, 0.5, 1.0 and 2.0 for both sets. Reagents were mixed in a ball mill for 12 hours, then melted at approximately 1600 °C in graphite crucibles for 2 hours under vacuum atmosphere (10^3 atm), this is done in order to remove completely OH^- molecules from glass structure, which present absorption band around 2.8 to 3.5 um.

This procedure was performed with a vacuum pump (Edwards, model RV8), which was connected to the furnace base. The furnace refrigeration was done using a water pump (Schneider, model BR2230), responsible to circulate the water from the reservoir, maintained about 50 Psi. When the vacuum pump is turned on, the optimal vacuum condition is achieved at approximately 1.32×10^{-5} atm, only then the furnace is turned on. In order to prevent any abrupt pressure variation the temperature is slowly increased by slowly increasing the current to the graphite

---

[1] The glasses were previously synthesized by the PhD student Giselly dos Santos Bianchi, under the supervision of Prof. Dr. Mauro Luciano Baesso.

resistors, so the reagents will not spread out. When the melting temperature is reached, the system is maintained at this temperature for about 2 hours. After that, the quenching is achieved by moving the crucible to a superior chamber, also maintained under vacuum atmosphere. The electric source is turned off and the batch cools down to room temperature. The glasses were then cut and polished for optical measurements.

3.2 Characterization

3.2.1 Density

The density ρ was determined by the Archimedes method [48] using a digital balance (Shimadzu, model AUW220D) and distilled water as the immersion liquid. The samples were firstly weighed in air, represented by m_{air}, then the apparent mass of the samples were measured when immersed in distilled water, m_{water}. Finally, glass densities can be calculated using the following expression

$$\rho_{\text{glass}} = \frac{m_{\text{air}}}{m_{\text{air}} - m_{\text{water}}} \rho_{\text{water}}, \tag{3.1}$$

where ρ_{glass} and ρ_{water} are the density of the glass and the density of the water, respectively. The latter is known from literature. The measurements were repeated five times for each sample. The mean values were calculated along with the respective standard deviations.

3.2.2 Refractive index

Refractive index n was determined using Brewster's angle method [49] at 442 and 632.8 nm, using a He-Cd (Kimmon Koha, model IK5652R-G) and a He-Ne (Newport, model R-32734) laser, respectively. The samples were placed over a goniometer that allows them to be rotated to a precise angular position. The laser beam is directed at the sample's surface in such a way that the polarization of the beam is perpendicular to the sample's rotation axis. Rotating the goniometer, the reflected beam intensity can be analyzed as a function of the rotation angle using a digital power meter (Thorlabs, model PM100D) and a photodiode (Thorlabs, model S121C). Figure 3.1 illustrates the behavior of the intensity of the reflected beam with the rotating angle. The angle at which the signal intensity is minimal is the

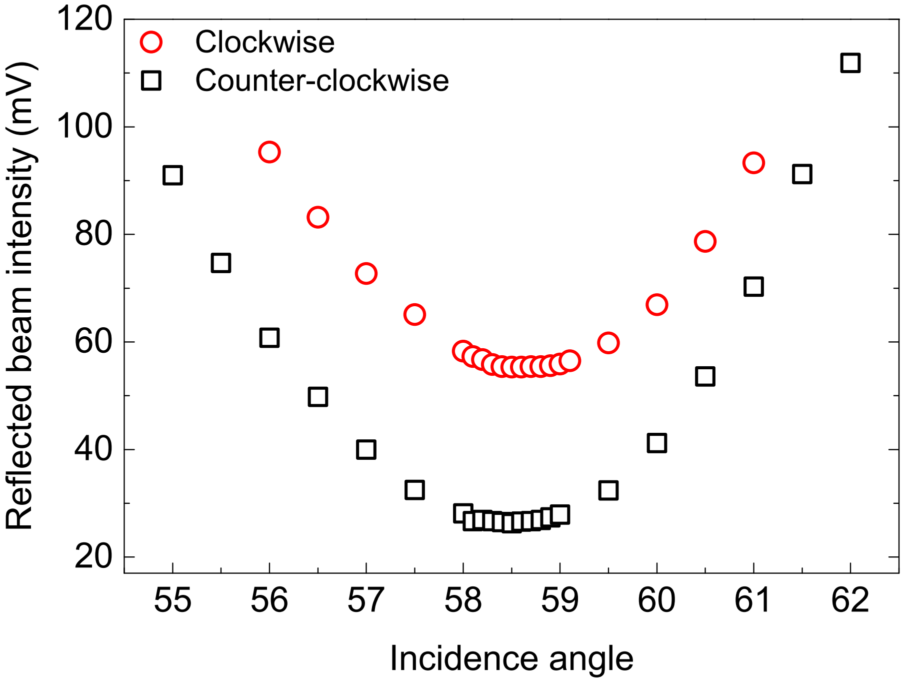

Figure 3.1: Illustration on the behavior of the intensity of the reflected beam with the rotating angle for both clockwise and counter-clockwise directions.

Brewster's angle and the refractive index can be calculated as follows

$$n = \tan(\theta_B), \tag{3.2}$$

where, n is the refractive index of the sample and θ_B is the Brewster's angle. The experiment is performed rotating the goniometer in the clockwise and counter-clockwise direction, as a way of minimizing any alignment errors. The value of θ_B is the mean value between both directions.

3.2.3 Absorption spectra

The experimental line strengths of the optical 4f-4f transitions of rare-earth elements are related to the area under the absorption band of the transitions (Eq. 2.1). For this reason, the absorption spectra of the samples were measured using an UV–VIS–NIR double beam spectrophotometer (Perkin-Elmer, model Lambda 900) in the spectral range of 300–2500 nm. To this end, the transmittance spectra were carried out for all samples and then converted to the absorption coefficient using the Beer–Lambert's law

$$I = I_0 e^{-\alpha l} \tag{3.3}$$

where, I_0 and I is the intensity before and after the beam passes through the sample; α is the optical absorption coefficient and l the optical path, which corresponds to the sample's thickness. The absorption coefficient is then given by

$$\alpha = -\frac{1}{l} \ln\left(\frac{I}{I_0}\right) \tag{3.4}$$

where $\frac{I}{I_0}$ is related to the transmittance measured with the spectrophotometer.

3.2.4 Photoluminescence spectra

The photoluminescence spectra were obtained using an Argon ion laser (Coherent, model Innova 90 Plus) tuned at 457 nm as excitation. The laser beam goes through the samples, which absorb part of its energy. This absorbed energy can be eliminated by different mechanisms, one of them is radiative emission. This happens because when electrons absorbs energy, they are promoted to excited levels and decay after some time. The emission in the visible region was collected by an optical fiber coupled to a monochromator (Newport, model 77780) and detected by a photomultiplier (Hamamatsu, model R1477). The signal was analyzed by a lock-in amplifier (Stanford Research System, model SR830). The upconversion spectra were obtained using the same arrangement of the visible emission, but the samples were excited using the 488 nm line of the Argon ion laser. In the infrared region, a He-Cd (Kimmon Koha, model IK5652R-G) at 442 nm was used as excitation, two quartz lenses collected the emission to monochromator which was detected by an InGaAs detector (NewPort, 70328NS). Figure 3.2 shows a schematic illustration of the experimental setup for the photoluminescence measurements.

3.2.5 Luminescence decay

The luminescence decay measurements were carried out using the same experimental arrangement of photoluminescence, but, instead of an Argon ion laser, the samples were excited by an optical parametric oscillator (OPO) (Surelite/Continuum) pumped by the third harmonic (355 nm) of a Nd-YAG laser (Surelite II/Continuum, 10 Hz, 5 ns). The emission signal was acquired by a digital oscilloscope (Tektronix,

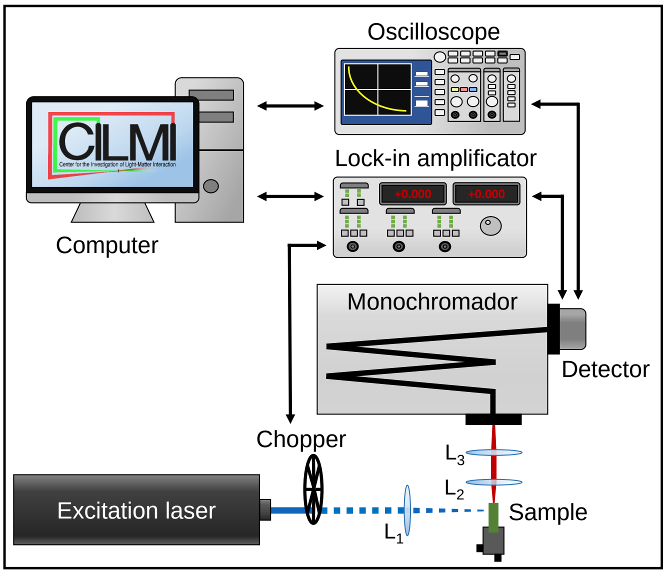

Figure 3.2: Schematic diagram showing the luminescence and luminescence decay experimental arrangements. L_n are lenses.

model DPO 4102B). An illustration[2] of the experimental arrangement for luminescence decay measurements is shown in Fig. 3.2.

The decay curves of the $^1D_2$ level (611 nm) were obtained with an OPO excitation at 586 nm; The decays curves of the $^3P_0$ level (488 nm) with excitation at 457 nm and the decay curves of the superposition of the $^1D_2$ and $^3P_0$ levels ($\sim$ 611 nm) were obtained with excitation at 488 nm.

---

[2] The illustration was kindly provided as courtesy by M.Sc. Anderson Gonçalves.

Chapter 4

Results and discussion

4.1 Density

Results for the density of the CAS and LSCAS glasses are presented in Fig. 4.1. No significant variation was observed in the densities of the studied glasses. The glass density measurements allow the calculation of the density of trivalent Praseodymium ions in the glass matrix, required to calculate the experimental line strength of the absorption bands (Eq. 2.1).

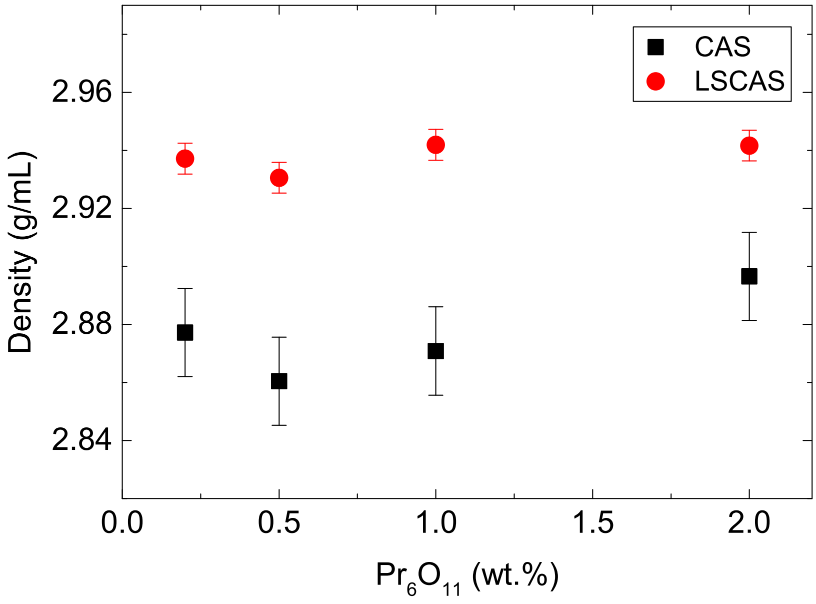

Figure 4.1: Density of the CAS and LSCAS glasses for different concentrations of dopant.

4.2 Refraction index

The refractive indexes obtained for CAS samples were 1.63 and 1.61 at 442 and 632.8 nm, respectively, while for LSCAS samples the refractive indexes were 1.68 and 1.66 at 442 and 632.8 nm, respectively. Results showed no significant variation in the refractive index with the Pr^{3+} concentration.

The Sellmeier's equation [50] was used to determine the refractive index as a function of the wavelength

$$n^2(\lambda) = 1 + \frac{A\lambda^2}{\lambda^2 - B}, \tag{4.1}$$

where λ is the wavelength and parameters A and B can be found solving the equation system. This result is important to get more precise values of the experimental line strength (Eq. 2.1), which depends on the refractive index of the mean wavelength of the optical transition. The refraction indexes calculated as a function the wavelength are shown in Figs 4.2 (CAS) and 4.3 (LSCAS). One can observe that the refractive indexes, for both glass hosts, present most significant variation with wavelength, roughly, in the visible range of the spectrum. On the over hand, in the infrared range, the refractive indexes vary only in the third decimal case.

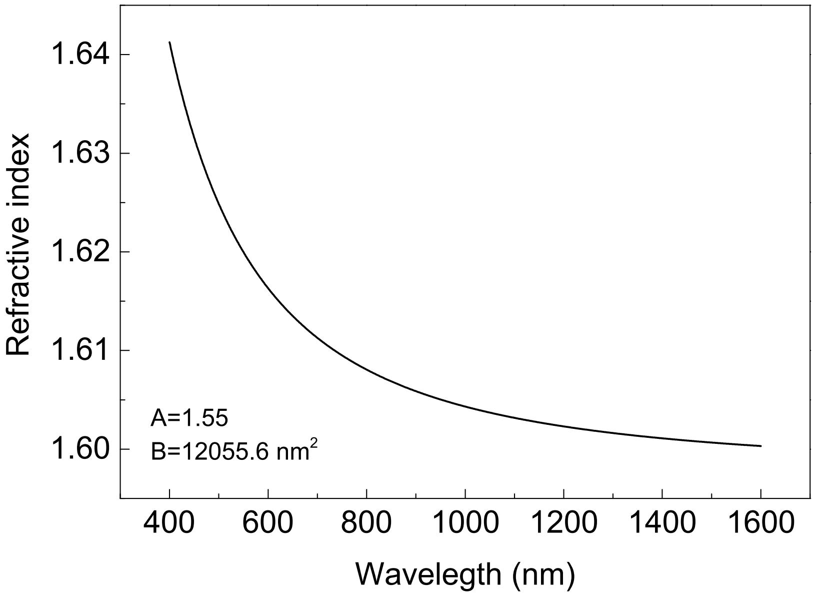

Figure 4.2: Refractive index as a function of the wavelength for the Pr^{3+}–doped CAS glasses. Values of the parameters A and B from Sellmeier's equation are indicated.

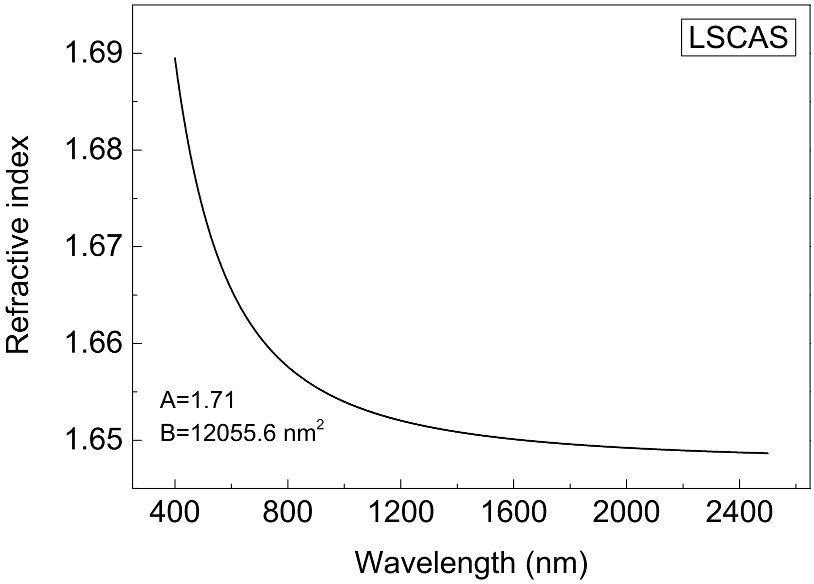

Figure 4.3: Refractive index as a function of the wavelength for th Pr^{3+}–doped LSCAS glasses. Values of the parameters A and B from Sellmeier's equation are indicated.

4.3 Absorption spectra

The absorption spectra for Pr^{3+}-doped CAS and LSCAS glasses in different concentrations of Pr^{3+} are shown in Figs. 4.4 and 4.5, respectively. In the range of 400 to 650 nm, the samples present four absorption bands related to transitions from the ground state $^3H_4$ to the $^3P_2$ (442 nm), $^3P_1$ (472 nm), $^3P_0$ (483 nm) and $^1D_2$ (588 nm) state. In the range of 900 to 2500 nm, samples present five more absorption bands corresponding to transitions from ground state $^3H_4$ to $^1G_4$ (999 nm), $^3F_4$ (1421 nm), $^3F_3$ (1504 nm), $^3F_2$ (1906 nm) and $^3H_6$ (2371 nm) state.

The absorption coefficient presented a linear increase as dopant concentration increases. Additionally, the band widths have not shown any displacement as dopant concentration increases, meaning all dopant inserted in the samples are homogeneously distributed.

In low Pr^3+ concentrations, some transitions are weak, for instance, $^3H_4 \rightarrow {}^1G_4$ and $^3H_4 \rightarrow {}^3H_6$ are barely noticeable in Figs. 4.4 and 4.5. As the calculation of experimental line strengths is related to the area of absorption band, low absorption values have direct influence in the uncertainty of the calculated value. Thus, absorption spectrum of high concentration provides most reliable values of S_{exp} [5]. Also for the LSCAS:0.2Pr^{3+} there was a significant difference in the IR range of the

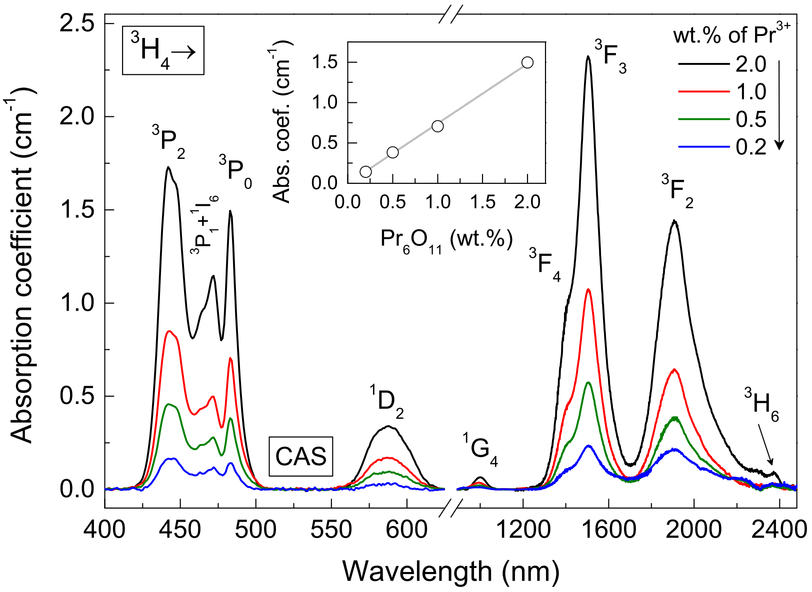

Figure 4.4: Optical absorption spectra of Pr^{3+}–doped CAS glasses in the UV–Vis–NIR range. Transitions are indicated. Inset shows absorption coefficient as a function of dopant concentration. The solid line is a guide to the eyes.

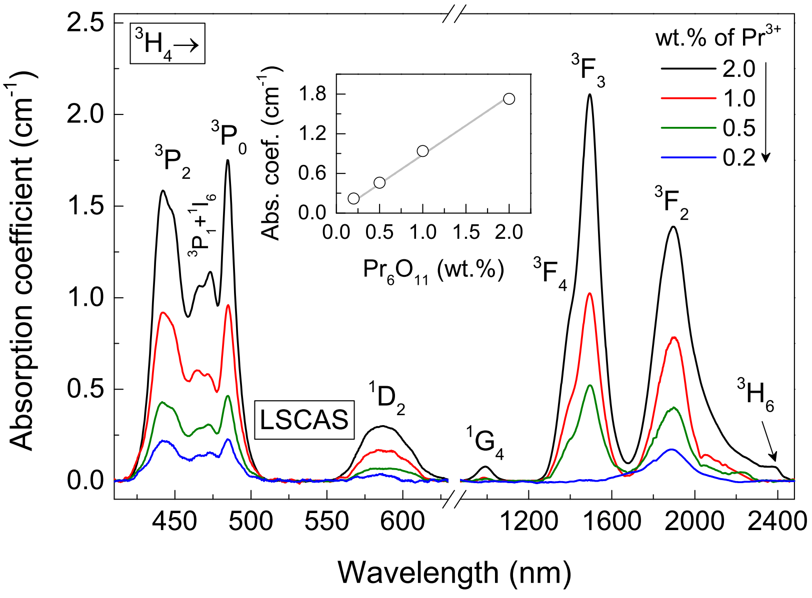

Figure 4.5: Optical absorption spectra of Pr^{3+}–doped LSCAS glasses in the UV–Vis–NIR range. Transitions are indicated. Inset shows absorption coefficient as a function of dopant concentration. The solid line is a guide to the eyes.

absorption spectrum, probably due to the very low intensity of the signal added with the fact this host presents crystallites, consequently causing light scattering which causes signal losses. In that case, no calculations were performed considering the LSCAS:0.2Pr^{3+}.

4.4 Emission spectra

The emission spectra of the CAS and LSCAS in the visible range, when excited at 457 nm, are shown in Figs. 4.6 and 4.7. The samples present a variety of emission bands, consisting of a broad blue band centered around 487 nm, a less intense green emission around 531 nm, a very broad and intense orange-red emission from 575 to 660 nm, and from 680 to 755 nm.

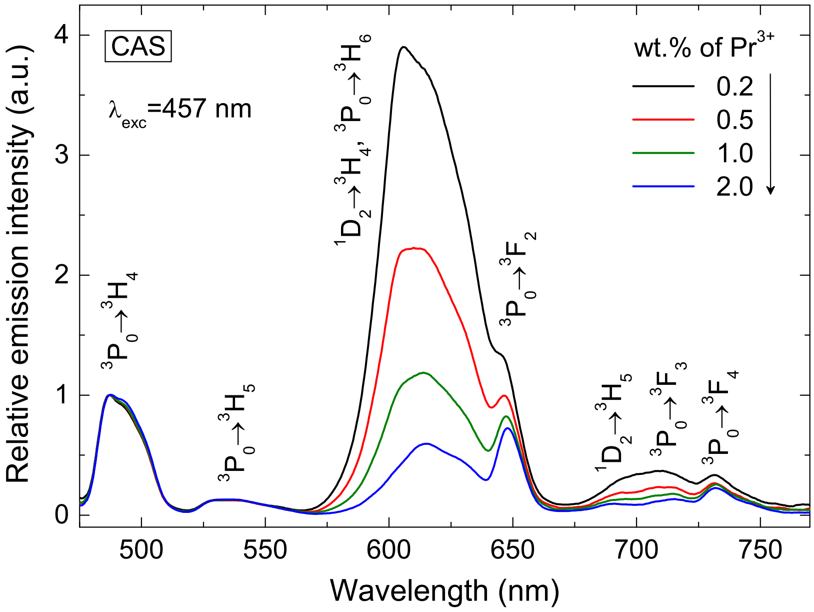

Figure 4.6: Relative emission spectra of Pr^{3+}–doped CAS glasses for different Pr^{3+} concentration. Transitions are indicated.

In order to investigate the changes in the emission induced by the Pr^{3+} concentration, Fig 4.6 shows the normalized emission by the intensity at 487 nm, for the CAS host. It is noticed a deviation of the peak position at 614 nm for the CAS:2.0Pr^{3+}, varying from 605 to 614 nm with the increasing of Pr^{3+} concentration. This can be explained by the superposition of two radiative transitions in this region. The ions in the fundamental level $^3H_4$ are excited to the upper $^3P_2$ level and quickly decay non-radiatively to the $^3P_0$ and $^1D_2$ levels. As a result, these excited ions transit

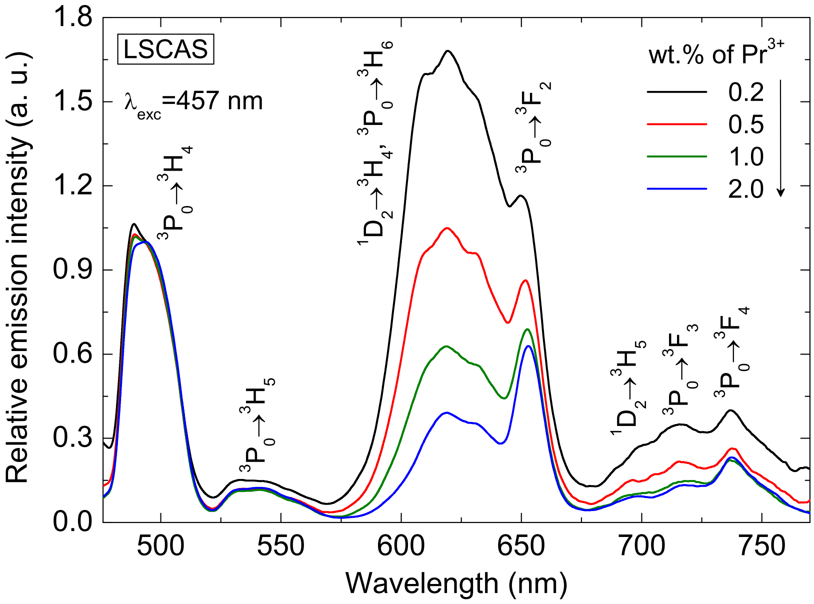

Figure 4.7: Relative emission spectra of Pr^{3+}–doped LSCAS glasses for different Pr^{3+} concentration. Transitions are indicated.

radiatively to the lower levels by photon emission, followed by non-radiative decays to the fundamental level by means of multiphonon relaxations. The energy levels diagram — presented in Fig. 4.8 — shows the blue and green emissions assigned to the $^3P_0 \rightarrow {}^3H_4$, $^3P_0 \rightarrow {}^3H_5$ transitions, respectively. The orange-red emissions are assigned to the $^1D_2 \rightarrow {}^3H_4$, $^3P_0 \rightarrow {}^3H_6$, $^3P_0 \rightarrow {}^3F_2$, $^1D_2 \rightarrow {}^3H_5$, $^3P_0 \rightarrow {}^3F_3$ and $^3P_0 \rightarrow {}^3F_4$ transitions.

As shown in the diagram, the transitions $^3P_0 \rightarrow {}^3H_6$ (614 nm) and $^1D_2 \rightarrow {}^3H_4$ (605 nm) are the transitions which overlap to emit from 575 to approximately 635 nm. The explanation for the deviation of the orange peak position is the relative increasing intensity of the $^3P_0 \rightarrow {}^3H_6$ transition while the $^1D_2 \rightarrow {}^3H_4$ transition intensity decreases for higher dopant concentrations, as already reported in the literature [13,14]. The $^1D_2 \rightarrow {}^3H_4$ emission, therefore, is more sensitive to the changes in the concentration compared to the $^3P_0 \rightarrow {}^3H_6$ emission. This may occur due to the cross-relaxation processes for the $^1D_2$ level, which are more favorable than the ones for the $^3P_0$ level [51,52].

For the LSCAS host, however, as one can observe in Fig 4.7, this deviation of the orange peak position is not observed, at least not as clear than in the CAS hosts. This is probably due to the different crystalline structure around the Pr^{3+} ions in the LSCAS, which has less silica content, causing differences in the emission spectra

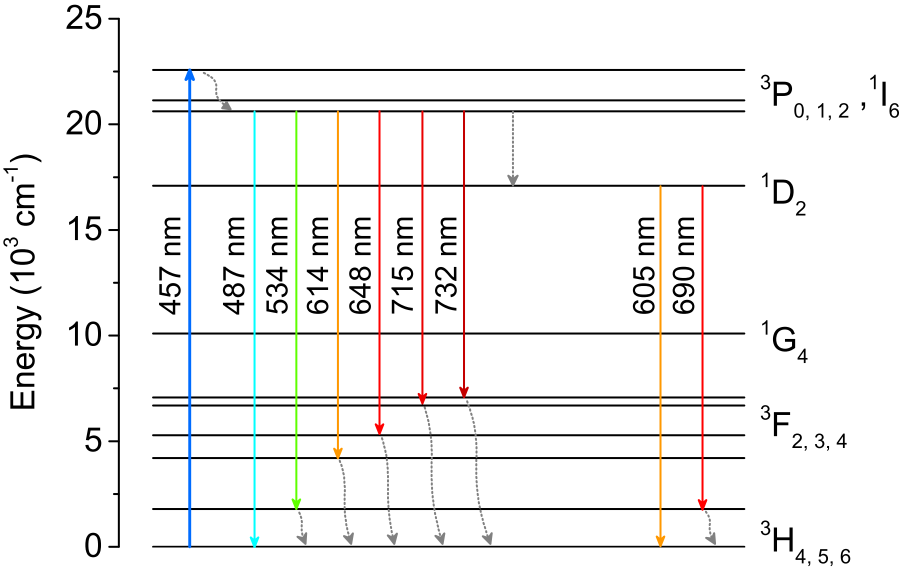

Figure 4.8: Energy levels of Pr^{3+} in CAS and LSCAS when excited at 457 nm.

that makes it harder to note any deviation in the orange peak.

Figures 4.6 and 4.7 also shows an unusual variation on the peak intensity of the $^3P_0 \rightarrow {}^3F_2$ emission with the dopant concentration when compared to the $^3P_0 \rightarrow {}^3H_6$ emission. Taking the ratio value between the intensity emission at 648 and 615 nm

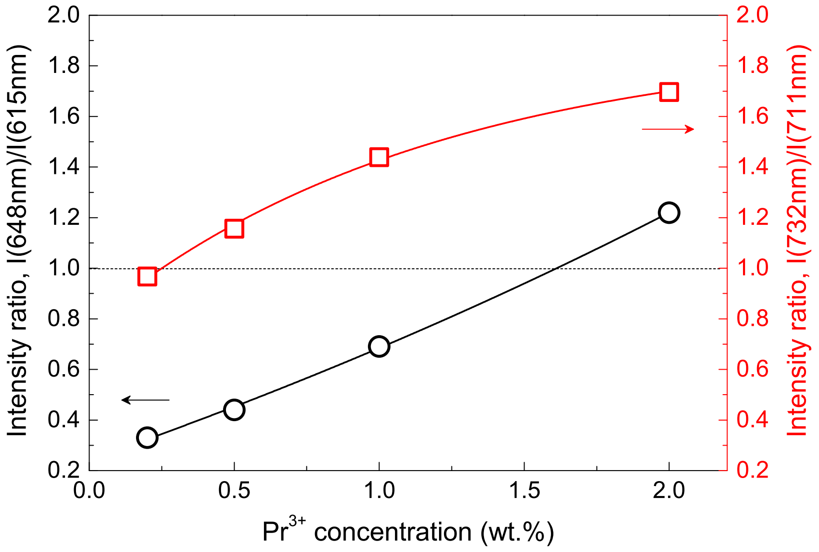

Figure 4.9: Intensity ratio between the $^3P_0 \rightarrow {}^3F_2$ and $^3P_0 \rightarrow {}^3H_6$ transitions (left), and intensity ratio between $^3P_0 \rightarrow {}^3F_4$ and $^3P_0 \rightarrow {}^3F_3$ transitions (right) in the CAS glass host. The solid lines are guides for the eye.

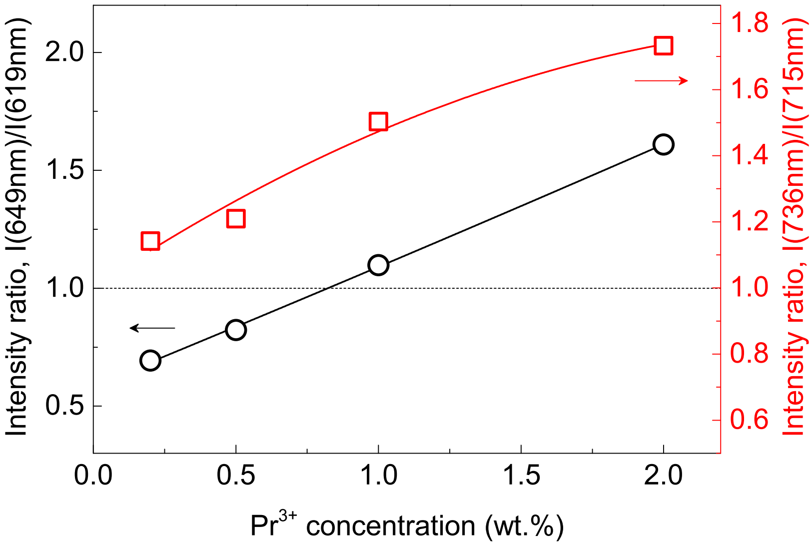

Figure 4.10: Intensity ratio between the $^3P_0 \rightarrow {}^3F_2$ and $^3P_0 \rightarrow {}^3H_6$ transitions (left), and intensity ratio between $^3P_0 \rightarrow {}^3F_4$ and $^3P_0 \rightarrow {}^3F_3$ transitions (right) in the LSCAS glass host. The solid lines are guides for the eye.

(CAS) or at 649 and 619 nm (LSCAS) it can be observed a relative increase in the $^3P_0 \rightarrow {}^3F_2$ emission, as shown in Figs. 4.9 (CAS) and 4.10 (LSCAS). This behavior suggests that the $^3P_0 \rightarrow {}^3F_2$ transition is hypersensitive [13, 35, 36]. This kind of transition is very sensitive to the environment surrounding the rare-earth ions and, in general, obeys the selection rules $|\Delta S| = 0$, $|\Delta L| \leq 0$ and $|\Delta J| \leq 2$, where S is the spin, L the orbital and J the spin-orbital quantum number. These are the same selection rules for the quadrupole transitions [53]. Notwithstanding, a relative intensity increase is even more evident when comparing the $^3P_0 \rightarrow {}^3F_4$ and $^3P_0 \rightarrow {}^3F_3$ transitions — corresponding to the peak position at 732 and 711 nm, respectively — of the CAS host, as shown in Fig. 4.9. As far as we are concerned, this result has not been reported in the literature yet. Despite the fact that this transition does not obey the selection rules, CAS:Pr^{3+} may be the first glass matrix to exhibit hypersensitivity in the $^3P_0 \rightarrow {}^3F_4$ transition. However, the same does not happen for the LSCAS host, as shown in Fig. 4.10, in this host the ratio value between the intensity emission of the $^3P_0 \rightarrow {}^3F_4$ and $^3P_0 \rightarrow {}^3F_3$ transitions — corresponding to the peak at 736 and 715 nm, respectively — present roughly the same proportion with the increasing of dopant concentration, meaning there was no relative intensity inversion in these transitions concerning the LSCAS host.

Figure 4.11 shows emission spectra in the IR range under 442 nm excitation.

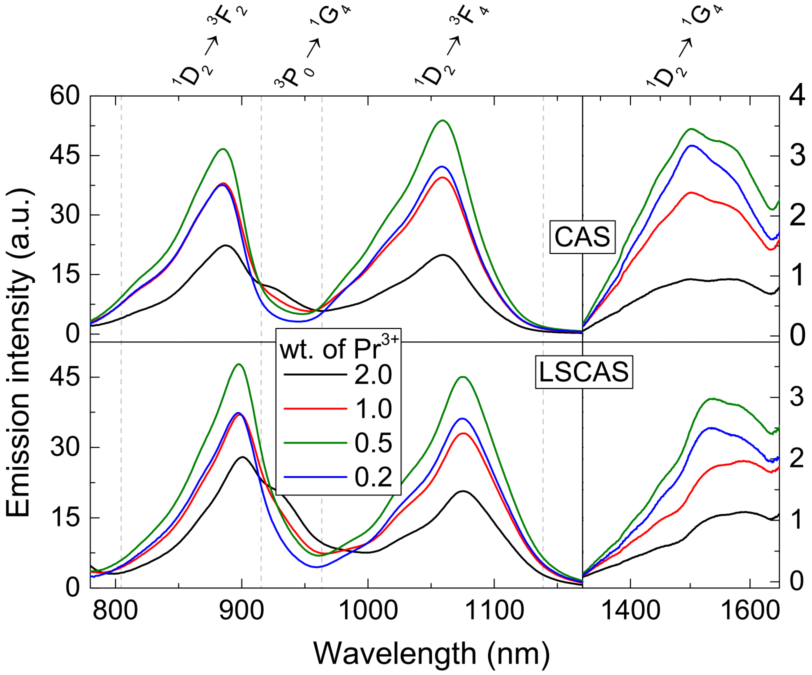

Figure 4.11: Emission spectra of Pr^{3+}–doped CAS and LSCAS glasses in the infra-red range under excitation at 442 nm. Transitions are indicated.

Three emission bands were observed around 890, 1060 and 1500 nm assigned to the $^1D_2 \rightarrow {}^3F_2$, $^3F_4$ and $^1G_4$ transitions, respectively. For higher concentrations, an additional band around 930 nm was noticed due the $^3P_0 \rightarrow {}^1G_4$ transition.

4.5 Luminescence time decay

The luminescence decay measurements were performed to obtain the lifetime constants for the $^3P_0$ and $^1D_2$ levels and to gather extra information about the non-exponential behavior already reported for Pr^{3+}–doped materials [1, 10, 54, 55]. This kind of behavior is associated to non-radiative transitions, which, in general, are interactions between OH^- groups and Pr^{3+} ions, related to self-quenching, to energy transfer through cross-relaxation processes [56] and related to migration of the excitation energy from one ion to another. However, interaction between OH^- groups cannot be the case for the samples presented in this work, since OH^- molecules have been removed during the glass synthesis. Therefore the OH^- group influence on the emission intensity can be neglected. Thus, the remaining possible explanations for the non-exponential behavior are energy transfer through cross-relaxations and migration of the excitation energy.

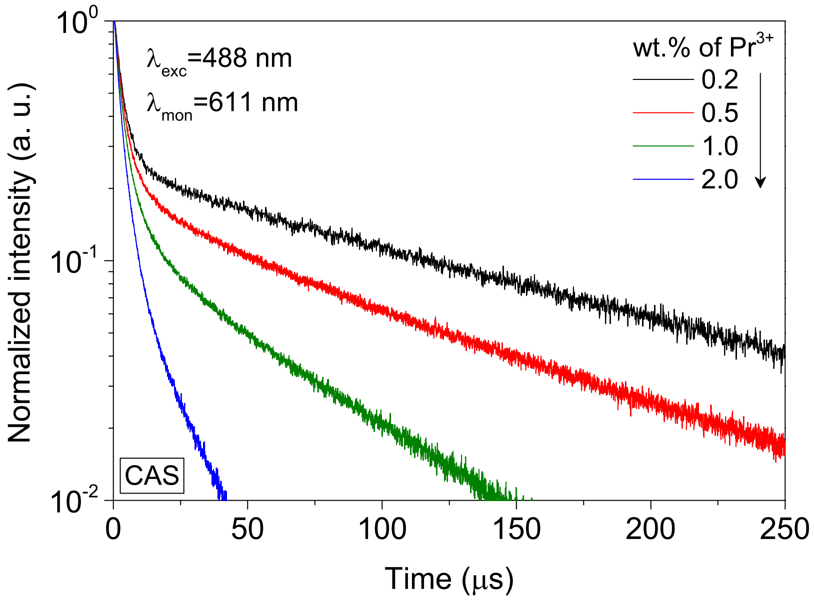

Figure 4.12: Luminescence decay curves on mono-log scale of Pr^{3+}–doped CAS excited at 488 nm and monitored at 611 nm, relative to the superposition of the $^1D_2 \rightarrow {}^3H_4$ and $^3P_0 \rightarrow {}^3H_6$ transitions.

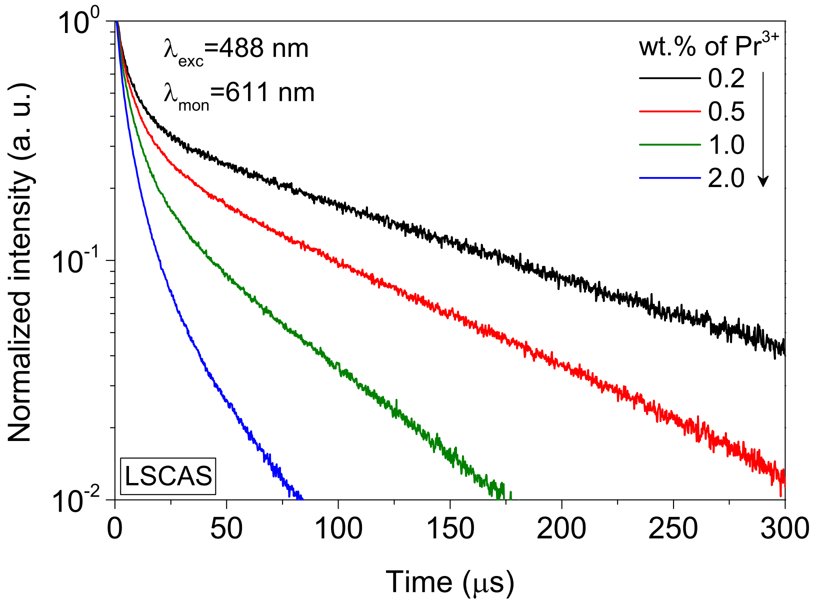

Figure 4.13: Luminescence decay curves on mono-log scale of Pr^{3+}–doped LSCAS excited at 488 nm and monitored at 611 nm, relative to the superposition of the $^1D_2 \rightarrow {}^3H_4$ and $^3P_0 \rightarrow {}^3H_6$ transitions.

In order to minimize any multiphonon relaxation process from the $^3P_2$ to the $^3P_0$ level, the samples were excited directly to the $^3P_0$ energy level using the OPO laser at 488 nm. Figures. 4.12 and 4.13 shows the time decay curves of the intensity emission at 611 nm for different concentrations of Pr^{3+}, for the CAS and LSCAS host, respectively. All decay curves presented non-exponential behavior. This behavior is even more evident for samples with higher doping concentration. This can be explained by the superposition of the $^3P_0 \rightarrow {}^3H_6$ and $^1D_2 \rightarrow {}^3H_4$ transitions [55], as already discussed in the previous section. The curves display two different trends; one short decay, typical of the $^3P_0$ level, and a slower decay, which is related to the $^1D_2$ level. This requires the use of a linear combination of two exponentials to fit the experimental data, which provides two lifetime constants, as presented in Tables 4.1 and 4.2, for the CAS and LSCAS hosts, respectively.

Table 4.1: Experimental lifetime constants of the CAS host for the $^3P_0$ (488 nm), $^1D_2$ (611 nm) and for the superposition of these levels (611 nm) with both short (τ_s) and long (τ_l) decay components of the double exponential fitting procedure as a function of Pr_6O_{11} content.

Pr_6O_{11}	$^3P_0$	$^3P_0$ & $^1D_2$		$^1D_2$
(wt.%)	(μs)	τ_s (μs)	τ_l (μs)	(μs)
0.2	2.6 ± 0.2	3.24 ± 0.01	154.2 ± 0.3	144.7 ± 0.2
0.5	2.5 ± 0.2	3.11 ± 0.01	80.9 ± 0.3	85.7 ± 0.2
1.0	2.3 ± 0.2	2.97 ± 0.01	48.4 ± 0.3	41.5 ± 0.2
2.0	2.1 ± 0.2	2.45 ± 0.01	19.5 ± 0.3	14.1 ± 0.2

Table 4.2: Experimental lifetime constants of the LSCAS host for the $^3P_0$ (488 nm), $^1D_2$ (611 nm) and for the superposition of these levels (611 nm) with both short (τ_s) and long (τ_l) decay components of the double exponential fitting procedure as a function of Pr_6O_{11} content.

Pr_6O_{11}	$^3P_0$	$^3P_0$ & $^1D_2$		$^1D_2$
(wt.%)	(μs)	τ_s (μs)	τ_l (μs)	(μs)
0.2	4.4 ± 0.2	6.96 ± 0.01	145.2 ± 0.3	138.2 ± 0.2
0.5	4.1 ± 0.2	6.94 ± 0.01	104.4 ± 0.3	87.8 ± 0.2
1.0	3.9 ± 0.2	5.77 ± 0.01	60.2 ± 0.3	44.2 ± 0.2
2.0	3.4 ± 0.2	3.88 ± 0.01	23.4 ± 0.3	16.5 ± 0.2

The superposition was confirmed by measuring separately the intensity decay of the $^1D_2 \rightarrow {}^3H_4$ and $^3P_0 \rightarrow {}^3H_4$ transitions. In Figs. 4.14 and 4.15, the luminescence decay the $^1D_2 \rightarrow {}^3H_4$ transition — for the CAS and LSCAS host, respectively — was monitored at 611 nm using the OPO laser at 586 nm as excitation, which promotes the ions directly to $^1D_2$ level. To determine the lifetime of the ions in $^3P_0$ level, the samples were excited at 457 nm and monitored at 488 nm, as shown in Figs. 4.16 and 4.17, for the CAS and LSCAS host, respectively. In order to obtain the lifetime constants, single-exponential fitting was not reliable for these decay curves, and alternative methods were considered. Fitting the curves with a linear combination of two [10, 54, 55] or three [1, 57] exponentials might solve the problem, but the lack of physical meaning of two or three lifetime constants, in these cases, is an issue to be considered. Stretched-exponential functions have been used to fit decay curves when the material has some kind of disorder [58, 59]. However, in this report we have performed the integration over the decay curves, resulting in the values shown in Tables 4.1 and 4.2, for the CAS and LSCAS host, respectively.

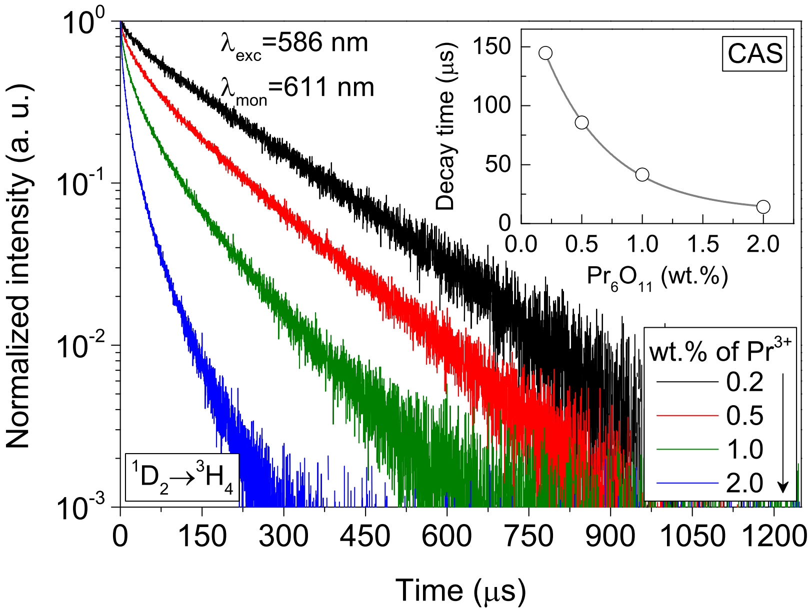

Figure 4.14: Luminescence decay curves on mono-log scale of the Pr^{3+}–doped CAS excited at 586 nm and monitored at 611 nm, relative to the $^1D_2 \rightarrow {}^3H_4$ transition.

The $^3P_0$ and $^1D_2$ levels present quite different lifetime constants. For the first, lifetime varied from (2.1 ± 0.2) μs for the CAS:2.0Pr^{3+} to (2.6 ± 0.2) μs for the CAS:0.2Pr^{3+} and from (3.4 ± 0.2) μs for the LSCAS:2.0Pr^{3+} to (4.4 ± 0.2) μs for the LSCAS:0.2Pr^{3+} while for the latter, lifetime varied from (14.1 ± 0.2) μs for the CAS:2.0Pr^{3+} to (144.7 ± 0.2) μs for the for the CAS:0.2Pr^{3+} and from (16.5

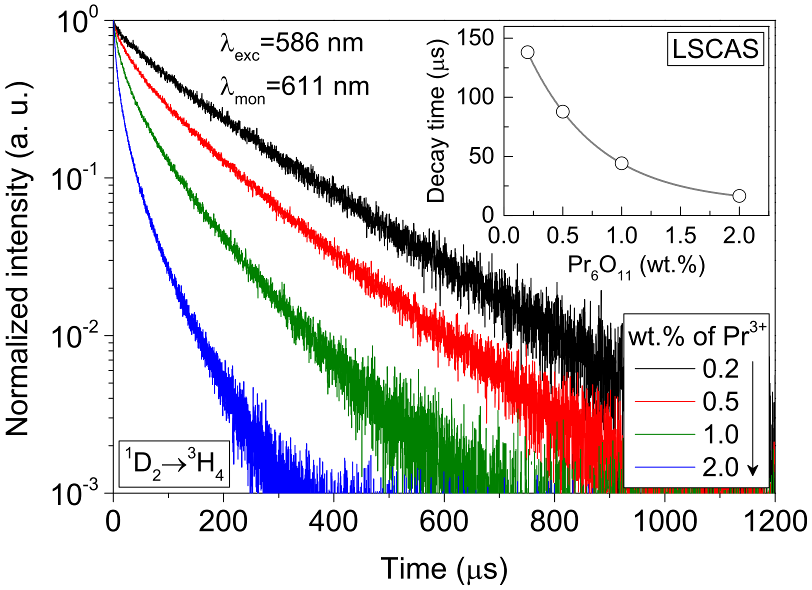

Figure 4.15: Luminescence decay curves on mono-log scale of the Pr^{3+}–doped LSCAS excited at 586 nm and monitored at 611 nm, relative to the $^1D_2 \rightarrow {}^3H_4$ transition.

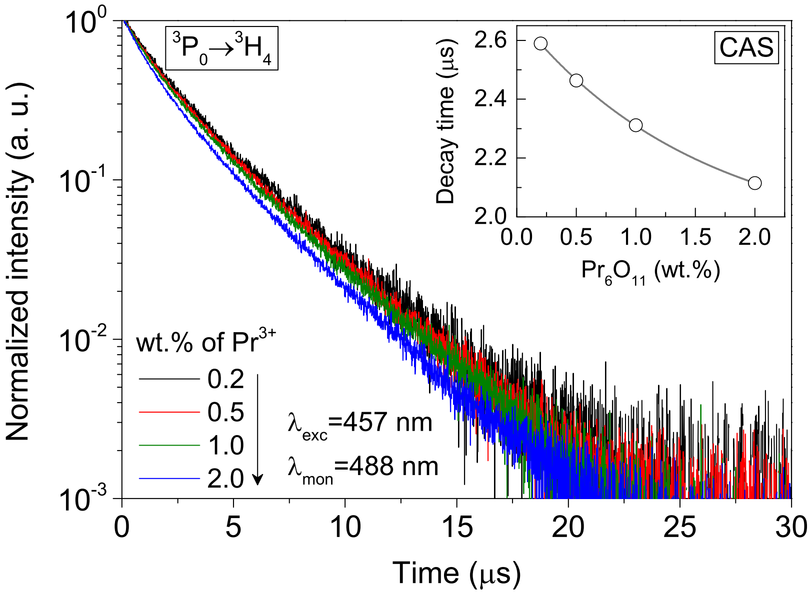

Figure 4.16: Luminescence decay curves on mono-log scale of the Pr^{3+}–doped CAS excited at 457 nm and monitored at 488 nm, relative to the $^3P_0 \rightarrow {}^3H_4$ transition.

± 0.2) μs for the LSCAS:2.0Pr^{3+} to (138.2 ± 0.2) μs for the LSCAS:0.2Pr^{3+}. This may be explained by different selection rules of each level, but also, by different

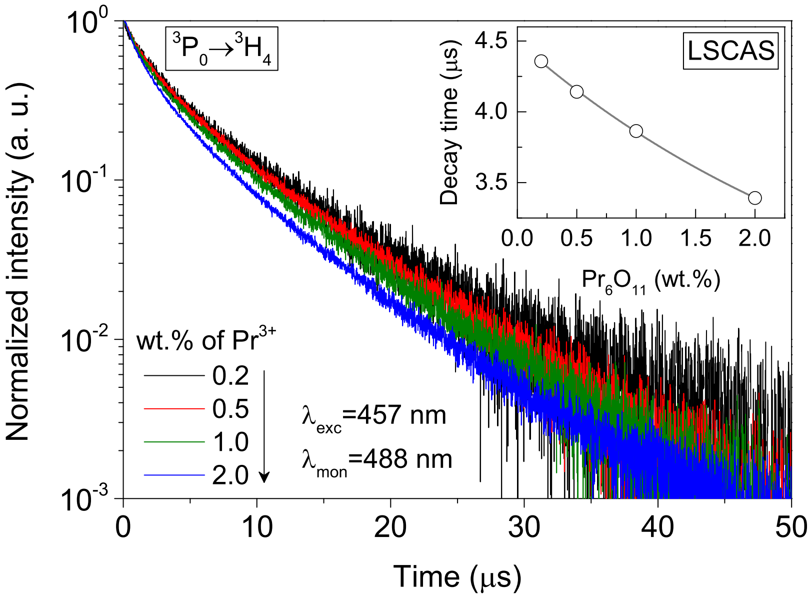

Figure 4.17: Luminescence decay curves on mono-log scale of the Pr^{3+}–doped LSCAS excited at 457 nm and monitored at 488 nm, relative to the $^3P_0 \rightarrow {}^3H_4$ transition.

population mechanisms [10], for instance, see Fig. 4.18. These lifetime constants are in agreement with the short and long components of the double exponential fitting showed in Tables 4.1 and 4.2.

All lifetime constants decrease with the increasing of dopant concentration, indicating concentration quenching caused by the reduction of the distances between Pr^{3+} ions, favoring non-radiative transitions [10]. Fig. 4.18 shows the possible cross-relaxation routes that may represent the concentration quenching [10, 51, 52].

4.6 Upconversion

Figures 4.19 and 4.20 shows the UV upconversion luminescence spectrum of the CAS:2.0Pr^{3+} and LSCAS:2.0Pr^{3+}, respectively, when excited in the $^3P_0$ level at 488 nm. In the CAS host, a broadband of approximately 84 nm from 256 nm to roughly 340 nm with maximum value at 270 nm is observed. This emission is in part in the UVC range, i.e., 100-280 nm. In the LSCAS host, a broadband of approximately 100 nm from 280 nm to roughly 380 nm with maximum value at 300 nm is observed. Although it is not difficult to find UVC emitters, such as mercury low-pressure vapor lamps which exhibit a very narrow (∼ 2 nm) emission

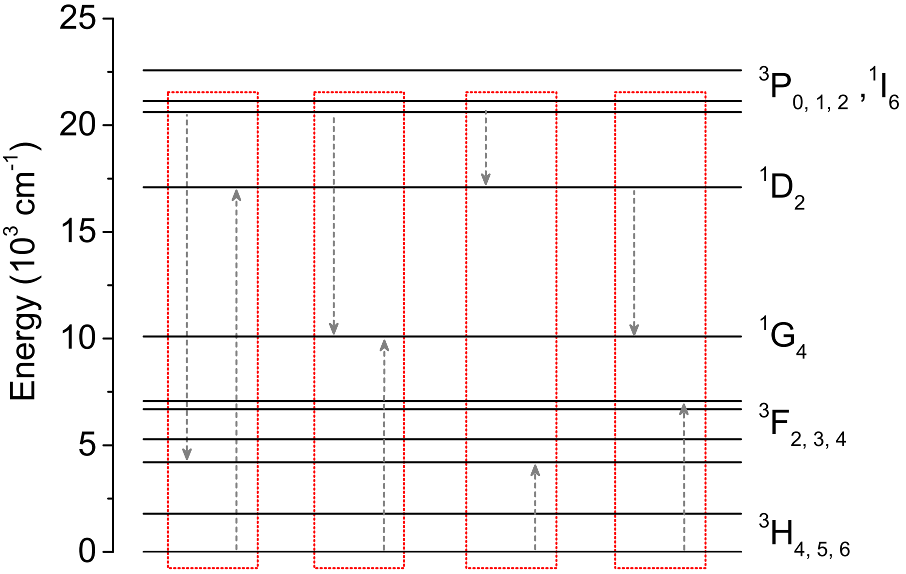

Figure 4.18: Representation of possible cross-relaxation routes for the $^3P_0$ and $^1D_2$ levels.

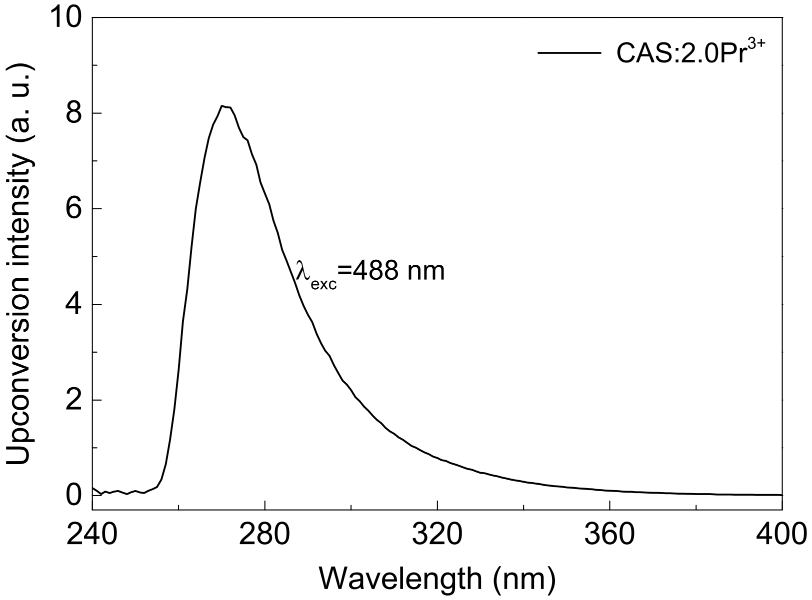

Figure 4.19: UV upconversion luminescence spectrum of CAS:2.0Pr^{3+} under excitation at 488 nm.

at 254 nm, it is not common to find broadband UVC emitters as the presented here.

There are several mechanisms that could be responsible for this process. The two most common processes involving the exchange of two low-energy photons by one high-energy photon are: (i) Excited state absorption (ESA), which is the absorption

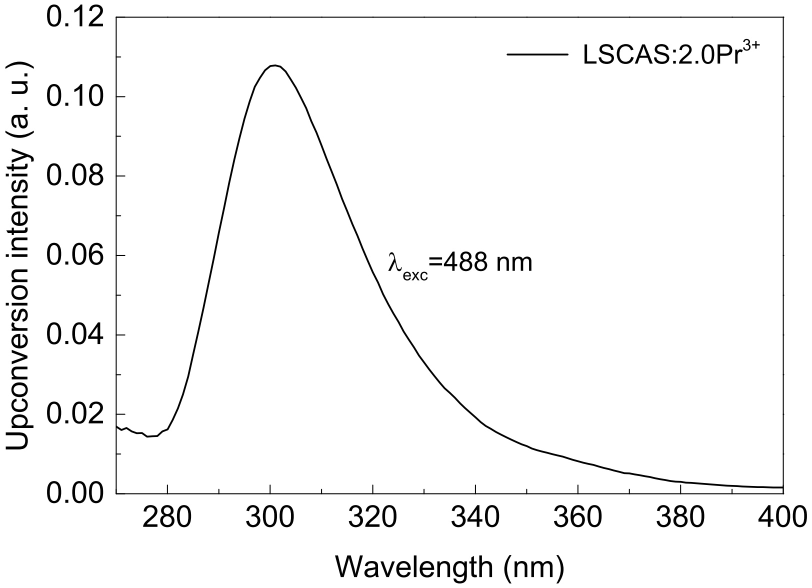

Figure 4.20: UV upconversion luminescence spectrum of LSCAS:2.0Pr^{3+} under excitation at 488 nm.

of a photon from the ground state to a higher intermediate state followed by an absorption of another photon in the intermediate state to an even higher state; (ii) Energy transfer upconversion (ETU), in which there are absorption of photons from ground to an intermediate state, then, two nearby ions interact non-radiatively exchanging their energy, whereas one of them is promoted to a higher excited level, and the other is transferred to a lower state. Both mechanisms are illustrated in Fig. 4.21.

In an upconversion process, emission intensity I and excitation power P are related by $I \propto P^n$, where n is the number of photons absorbed for each photon emitted [60]. To elucidate the origin of this energy upconversion we have measured the luminescence peak intensity at 270 nm and 300 nm, for the CAS and LSCAS host, respectively, as a function of the pump power, and the results are presented in double-logarithmic scale in Figs. 4.22 and 4.23, for the same hosts, respectively, along with the respective linear fit. Generally speaking, in an upconversion process involving at least n photons, n is the smallest integer greater than the slope value [61]. Results in this work showed a slope varying from 1.45 ± 0.02 to 1.78 ± 0.02, for the CAS:0.2Pr^{3+} and CAS:2.0Pr^{3+}, respectively, and from 1.15 ± 0.02 to 1.36 ± 0.02, for the LSCAS:2.0Pr^{3+} and LSCAS:1.0Pr^{3+}, respectively. Such values of the slope asserts the two-photon upconversion.

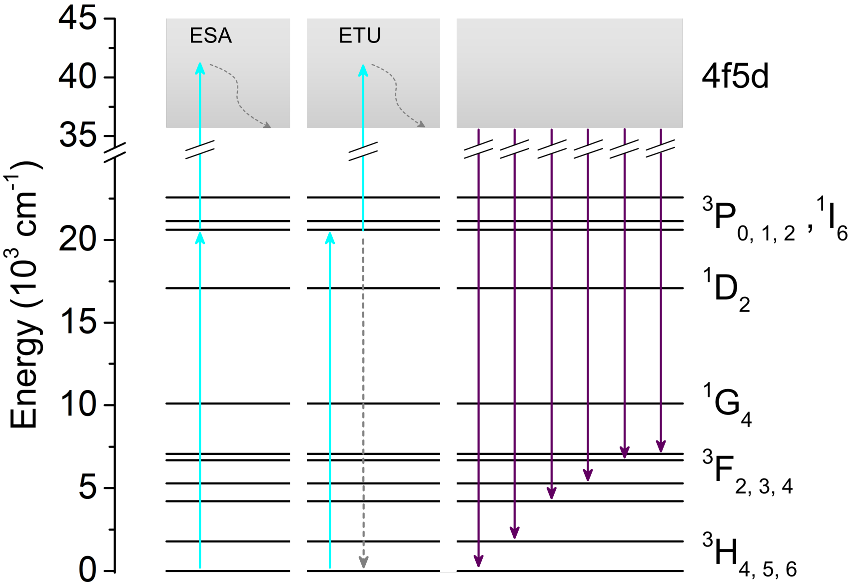

Figure 4.21: Illustration of the possible upconversion mechanisms: excited state absorption (ESA) and energy transfer upconversion (ETU). Solid arrows show absorption/emission of radiation and dashed arrows shows non-radiative transitions.

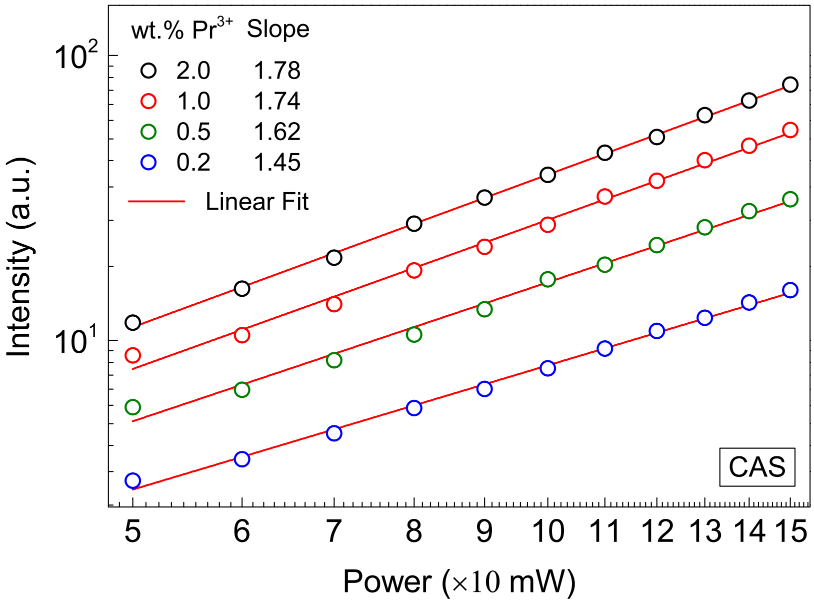

Figure 4.22: Peak intensity at 270 nm of the upconversion emission of the CAS host as a function of excitation power.

In order to distinguish whether the dominant mechanism is ETU or ESA, analysis of the upconversion lifetime were performed taking into account the populating

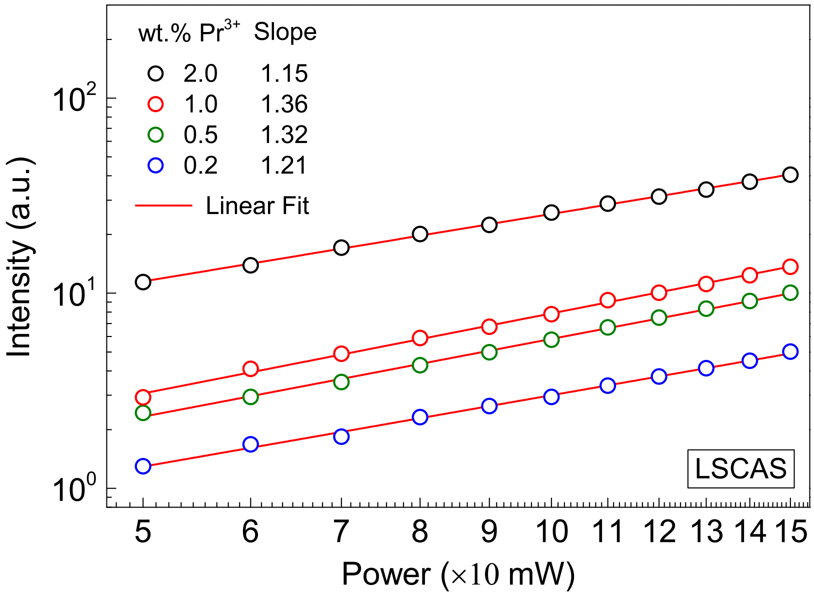

Figure 4.23: Peak intensity at 300 nm of the upconversion emission of the LSCAS host as a function of excitation power.

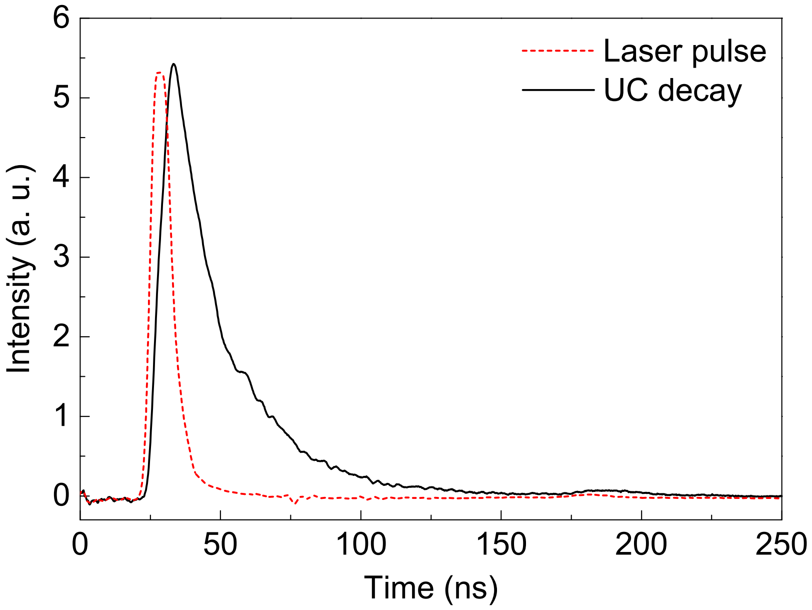

Figure 4.24: Luminescence decay of the upconverted emission of CAS host along with the laser pulse. The luminescence reaches the maximum intensity when almost all pulse energy is delivered. For the LSCAS host, behavior is similar.

period. In an ESA process, the rising of the upconversion is limited to the duration of the pulse, since the pulse is the only source populating the upper state. Conversely, in an ETU process, the upper state is populated indirectly by the pulse, by means of the energy transfer between ions in the lower state. This process may generate a delay on the rising period of the upconversion, depending on how fast the energy transfer process occur. Measurements of the laser pulse, along with the upconversion decay were performed and the curves are presented in Fig. 4.24. The results show that the rising of the UC emission reaches a maximum value when approximately all energy of the pulse is delivered. This observation does not clarify if the upconversion mechanism is either ESA or ETU, because the energy transfer processes may be as fast as the pulse duration.

The special relevance of this emission is that, for the CAS host, it covers the UVC range (254–280 nm) which is known for its potential antimicrobial use [31, 62]. The use of an optical device with an UVC emitting side is of great benefit for health institutions or biologic laboratories since they demand highly sterilized areas which could be performed without handling hazardous chemicals. Furthermore, an UVC emitting container could be used as a tool to disinfect water in remote places, using only the sunlight (blue radiation) as a source of the upconversion leading the UVC radiation.

4.7 Judd–Ofelt analysis

Experimental line strengths for the transitions were calculated according to Eq. 2.1 and are presented in Table 4.3.

Table 4.3: Experimental line strengths S_{exp} (10^{-20} cm^2) for CAS and LSCAS glasses for different concentrations of Pr^{3+} in wt.%.

	CAS:xPr^{3+}			LSCAS:xPr^{3+}		
Transition	0.5	1.0	2.0	0.5	1.0	2.0
$^3H_4 \rightarrow$						
$^3P_2$	8.06	7.40	7.32	7.76	8.26	6.80
$^3P_1$	3.63	3.29	3.64	4.21	4.23	3.88
$^3P_0$	3.29	3.02	3.00	4.33	4.44	3.82
$^1D_2$	2.05	1.83	1.75	1.53	1.82	1.72
$^1G_4$	0.75	0.55	0.42	0.25	0.14	0.65
$^3F_4$+$^3F_3$	23.91	21.73	23.55	20.70	19.19	20.29
$^3F_2$+$^3H_6$	18.52	14.61	16.96	17.14	14.88	16.32

Using the values of the experimental line strengths, the matrix elements for Pr^{3+}

— listed in Ref. [46] — and employing least squares method, the J–O parameters were derived from standard and modified theories. Calculations were performed considering two situations: the $^3H_4 \rightarrow {}^1I_6$ transition is convoluted in the band associated to the (i) $^3H_4 \rightarrow {}^3P_1$ and (ii) $^3H_4 \rightarrow {}^3P_2$ transitions [46], referred as CAS1/LSCAS1 and CAS2/LSCAS2, respectively.

Table 4.4: Results for the calculated line strength S_{cal}, intensity parameters Ω_λ and root mean square deviation δ_{rms} (all in units of 10^{-20} cm^2) for the CAS hosts using the standard theory for different concentrations of Pr^{3+} in wt.%.

	Standard S_{cal}					
	CAS1:xPr^{3+}			CAS2:xPr^{3+}		
Transition	0.5	1.0	2.0	0.5	1.0	2.0
$^3H_4 \rightarrow$						
$^3P_2$	2.53	2.34	2.51	3.84	3.50	3.75
$^3P_1$	3.95	3.58	3.81	3.84	3.50	3.64
$^3P_0$	2.80	2.56	2.70	3.82	3.48	3.62
$^1D_2$	1.00	0.91	0.98	1.00	0.91	0.98
$^1G_4$	0.27	0.24	0.26	0.27	0.24	0.26
$^3F_4+^3F_3$	24.62	22.37	24.16	24.53	22.29	24.06
$^3F_2+^3H_6$	18.40	14.51	16.86	18.50	14.59	16.94
Ω_2	14.91	8.96	12.38	10.90	5.34	8.76
Ω_4	16.35	14.96	15.79	22.30	20.33	21.14
Ω_6	14.14	13.13	14.12	12.33	11.5	12.48
δ_{rms}	2.86	2.61	2.46	2.23	2.04	1.87

Results from the standard J–O theory are presented in Tables 4.4 and 4.5, for the CAS and LSCAS hosts, respectively. All calculated intensity parameters presented positive values and reasonable values for δ_{rms} [9, 14, 63]. Nevertheless, many reports have indicated the standard theory is not the optimal theory for Pr^{3+}-doped materials, which makes it necessary to examine the accuracy of these results and to compare it with modified theories.

Incidentally, in Tables 4.4 and 4.5, CAS2 and LSCAS2 sets presented the lowest root mean square deviation for all concentrations, the same occurred to the modified theories, consequently, all following results correspond to these sets.

Calculations from Kornienko *et al.* method exhibited same behavior for all concentrations, thus, by simplicity, only results for 2.0 wt.% of Pr^{3+} are shown in Table 4.6. Some authors suggest to adopt an expected value of 10^{-5} cm for the

Table 4.5: Results for the calculated line strength S_{cal}, intensity parameters Ω_λ and root mean square deviation δ_{rms} (all in units of 10^{-20} cm^2) for the LSCAS hosts using the standard theory for different concentrations of Pr^{3+} in wt.%.

	Standard S_{cal}					
	LSCAS1:xPr^{3+}			LSCAS2:xPr^{3+}		
Transition	0.5	1.0	2.0	0.5	1.0	2.0
$^3H_4 \rightarrow$						
$^3P_2$	2.16	2.03	2.12	3.55	3.40	3.40
$^3P_1$	4.78	4.82	4.34	4.65	4.77	4.16
$^3P_0$	3.54	3.62	3.19	4.62	4.74	4.14
$^1D_2$	0.87	0.82	0.85	0.87	0.82	0.85
$^1G_4$	0.23	0.21	0.23	0.23	0.21	0.22
$^3F_4$+$^3F_3$	21.40	19.97	20.89	21.30	19.88	20.79
$^3F_2$+$^3H_6$	17.02	14.75	16.22	17.11	14.85	16.30
Ω_2	10.4	6.14	10.51	6.18	1.70	6.77
Ω_4	20.7	21.12	18.63	27.00	27.70	24.16
Ω_6	10.3	9.23	10.54	8.36	7.24	8.85
δ_{rms}	2.88	3.22	2.44	2.17	2.52	1.80

parameter $\mathcal{A}$, not letting it vary [3, 12, 45]. With this consideration, the results are quite inferior than those of standard theory, presenting deviations δ_{rms} up to three times greater (second and fourth columns of Table 4.6). On the other hand, better fitting results were achieved with $\mathcal{A} \sim 10^{-7}$ cm for all samples, leading fairly good agreement between experimental and calculated line strengths. The deviations δ_{rms} are about the same as those of standard theory (third and fifth columns of Table 4.6). However, this magnitude of $\mathcal{A}$ is rather unreal since it corresponds to an energy of the 4f5d configuration of 5×10^6 cm^{-1}, which is clearly erroneous. Generally speaking, this modified theory can lead reasonable agreement between experimental and calculated line strengths, but making use of an additional parameter that may induce, at least in the present work, unphysical aspects.

By the approach of Flórez *et al.*, several sets of parameters were calculated and the best set would be the one which obeys the following requirements: (i) all intensity parameters must be positive and (ii) the root mean square must be the lowest. Differently than the work of Flórez *et al.* [46], where only one combination of parameters produced positive values for all intensity parameters Ω_k, results in this work presented a considerable amount of sets with all positive Ω_k. Table 4.7 shows

Table 4.6: Results for the calculated line strength S_{cal}, intensity parameters Ω_λ and root mean square deviation δ_{rms} (all in units of 10^{-20} cm^2) for the CAS and LSCAS hosts using the Kornienko *et al.* modified theory for different concentrations of Pr^{3+} in wt.%.

	Kornienko *et al.* S_{cal}			
	CAS2:2.0Pr^{3+}		LSCAS2:2.0Pr^{3+}	
Transition	2.0	2.0	2.0	2.0
$^3H_4 \rightarrow$				
$^3P_2$	4.78	3.76	4.28	3.41
$^3P_1$	3.44	3.64	3.97	4.16
$^3P_0$	3.43	3.62	3.95	4.14
$^1D_2$	1.31	0.98	1.12	0.85
$^1G_4$	0.35	0.26	0.31	0.23
$^3F_4$+$^3F_3$	32.30	24.12	27.84	20.84
$^3F_2$+$^3H_6$	24.05	17.00	23.12	16.35
Ω_2	20.41	8.84	18.32	6.85
Ω_4	20.01	21.13	23.08	24.15
Ω_6	18.98	12.53	14.34	8.89
δ_{rms}	5.78	1.87	5.25	1.80
$\mathcal{A}$	10^{-5}	10^{-7}	10^{-5}	10^{-7}

the calculated line strengths and respective values of Ω_k for the combination with lowest root mean square, which are k = 2, 3, 4, 6 for both glass hosts. The inclusion of the odd parameter has led a significantly better agreement between experimental and calculated line strengths. The deviations δ_{rms} were at least two times lower than the standard theory, although the contribution of the odd parameter Ω_3 is rather high.

Nevertheless, a better insight about the consistency of these results is obtained comparing the spectroscopic properties from both the standard and the Flórez *et al.* modified theory. Results for the emission transition probabilities, branching ratios and radiative lifetimes for CAS and LSCAS with 0.5, 1.0 and 2.0 wt.% of Pr^{3+} are shown in Tables 4.8, 4.9 and 4.10, respectively. Emission spectra in Figs 4.6, 4.7 and 4.11 show a significantly better agreement to the standard J–O theory rather than the modified theory of Flórez *et al.*. For instance, the two most intense emission transitions in visible range, according to standard theory, would be the $^3P_0 \rightarrow {}^3H_4$ and $^3P_0 \rightarrow {}^3F_2$ for both glass hosts, while for the modified theory, results suggest the $^3P_0 \rightarrow {}^3F_3$ and $^3H_4$ transitions would be the two most intense for both hosts,

Table 4.7: Results for the calculated line strength S_{cal}, intensity parameters Ω_λ and root mean square deviation δ_{rms} (all in units of 10^{-20} cm^2) for the CAS and LSCAS hosts the Flórez *et al.* modified theory for different concentrations of Pr^{3+} in wt.%.

	Flórez *et al.* S_{cal}					
	CAS2:xPr^{3+}			LSCAS2:xPr^{3+}		
Transition	0.5	1.0	2.0	0.5	1.0	2.0
$^3H_4 \rightarrow$						
$^3P_2$	7.98	7.33	7.26	7.70	8.18	6.73
$^3P_1$	3.48	3.17	3.34	4.29	4.35	3.87
$^3P_0$	3.46	3.15	3.32	4.27	4.33	3.85
$^1D_2$	0.73	0.66	0.75	0.60	0.50	0.63
$^1G_4$	0.21	0.18	0.21	0.17	0.14	0.18
$^3F_4$+$^3F_3$	23.99	21.79	23.60	20.76	19.26	20.35
$^3F_2$+$^3H_6$	18.51	14.61	16.95	17.13	14.88	16.32
Ω_2	15.31	9.41	12.49	10.60	6.79	10.31
Ω_3	767.91	709.04	649.90	769.33	886.36	617.25
Ω_4	20.22	18.40	19.38	24.90	25.29	22.49
Ω_6	7.31	6.87	8.23	3.33	1.45	4.81
δ_{rms}	0.84	0.72	0.65	0.55	0.77	0.69

which is in disagreement with the experimental emission spectra.

Moreover, regarding radiative lifetimes, standard theory also presents a better agreement to experimental lifetimes τ_{exp}. With the theoretical and experimental radiative lifetime, the emission quantum efficiency is given by

$$\eta = \frac{\tau_{exp}}{\tau}. \tag{4.2}$$

Considering the values obtained by standard theory, the emission quantum efficiencies of CAS:2.0Pr^{3+} for the $^1D_2$ and $^3P_0$ levels were 0.24 and 0.31, respectively. For LSCAS:2.0Pr^{3+}, the emission quantum efficiencies for these levels were 0.30 and 0.56, respectively. One the other hand, the results with modified theory of Flórez *et al.* for the emission quantum efficiencies of CAS:2.0Pr^{3+} were 3.32 and 1.74 for $^1D_2$ and $^3P_0$ levels, respectively. For LSCAS:2.0Pr^{3+} were 2.48 and 3.00 for the same levels, respectively. Same behavior is present in other concentrations of dopant. Emission quantum efficiency values over 1 are, in general, related to some energy transfer mechanisms. Nevertheless, the concentration of 2.0 wt.% of Pr^{3+} should be close to quenching concentration, which decreases the emission quantum

Table 4.8: Emission transition probabilities, A (s^{-1}), branching ratios, β, and radiative lifetimes, τ (μs), from standard and Flórez *et al.* J–O theory and experimental radiative lifetimes, τ_{exp} (μs), for CAS and LSCAS with 0.5 wt.% of Pr^{3+}.

	CAS2:0.5Pr^{3+}				LSCAS2:0.5Pr^{3+}			
	Standard		Flórez *et al.*		Standard		Flórez *et al.*	
Transition	A	β	A	β	A	β	A	β
$^3P_0 \rightarrow$								
$^3H_4$	93728	0.594	84970	0.088	123920	0.691	114335	0.107
$^3H_5$	0	0	0	0	0	0	0	0
$^3H_6$	10656	0.068	6315	0.007	7781	0.043	3097	0.003
$^3F_2$	32527	0.206	45692	0.047	20220	0.113	34681	0.032
$^3F_3$	0	0	808925	0.838	0	0	895135	0.835
$^3F_4$	16739	0.106	15175	0.016	21966	0.122	20267	0.019
$^1G_4$	4119	0.026	3734	0.004	5494	0.031	5069	0.005
	$\tau = 6.34$ μs		$\tau = 1.04$ μs		$\tau = 5.58$ μs		$\tau = 0.93$ μs	
	$\tau_{\text{exp}} = (2.5 \pm 0.2)$ μs				$\tau_{\text{exp}} = (4.1 \pm 0.2)$ μs			
$^1D_2 \rightarrow$								
$^3H_4$	11370	0.627	11235	0.041	13947	0.721	13800	0.047
$^3H_5$	86	0.005	6507	0.024	107	0.006	6953	0.024
$^3F_2$	2703	0.149	11111	0.040	2768	0.143	12076	0.041
$^3F_4$	3166	0.175	185428	0.670	1903	0.098	194036	0.662
$^1G_4$	799	0.044	62503	0.226	618	0.032	66155	0.226
	$\tau = 55.17$ μs		$\tau = 3.61$ μs		$\tau = 51.69$ μs		$\tau = 3.41$ μs	
	$\tau_{\text{exp}} = (85.7 \pm 0.2)$ μs				$\tau_{\text{exp}} = (87.8 \pm 0.2)$ μs			

Table 4.9: Emission transition probabilities, A (s^{-1}), branching ratios, β, and radiative lifetimes, τ (μs), from standard and Flórez *et al.* J–O theory and experimental radiative lifetimes, τ_{exp} (μs), for CAS and LSCAS with 1.0 wt.% of Pr^{3+}.

	CAS2:1.0Pr^{3+}				LSCAS2:1.0Pr^{3+}			
	Standard		Flórez *et al.*		Standard		Flórez *et al.*	
Transition	A	β	A	β	A	β	A	β
$^3P_0 \rightarrow$								
$^3H_4$	85416	0.656	77329	0.088	127138	0.759	116095	0.097
$^3H_5$	0	0	0	0	0	0	0	0
$^3H_6$	9942	0.076	5934	0.007	6742	0.040	1346	0.001
$^3F_2$	15939	0.122	28095	0.032	5554	0.033	22215	0.019
$^3F_3$	0	0	746911	0.853	0	0	1031300	0.862
$^3F_4$	15254	0.117	13810	0.016	22536	0.134	20579	0.017
$^1G_4$	3754	0.029	3398	0.004	5636	0.034	5147	0.004
	$\tau = 7.67$ μs		$\tau = 1.14$ μs		$\tau = 5.97$ μs		$\tau = 0.84$ μs	
	$\tau_{\text{exp}} = (2.3 \pm 0.2)$ μs				$\tau_{\text{exp}} = (3.9 \pm 0.2)$ μs			
$^1D_2 \rightarrow$								
$^3H_4$	10368	0.712	10243	0.040	14086	0.807	13916	0.042
$^3H_5$	79	0.005	6007	0.024	109	0.006	7997	0.024
$^3F_2$	1961	0.135	9725	0.038	2280	0.131	13004	0.039
$^3F_4$	1604	0.110	169894	0.671	573	0.033	221933	0.667
$^1G_4$	529	0.036	57502	0.227	401	0.023	75907	0.228
	$\tau = 68.76$ μs		$\tau = 3.95$ μs		$\tau = 57.31$ μs		$\tau =3.01$ μs	
	$\tau_{\text{exp}} = (41.5 \pm 0.2)$ μs				$\tau_{\text{exp}} = (44.2 \pm 0.2)$ μs			

Table 4.10: Emission transition probabilities, A (s^{-1}), branching ratios, β, and radiative lifetimes, τ (μs), from standard and Flórez *et al.* J–O theory and experimental radiative lifetimes, τ_{exp} (μs), for CAS and LSCAS with 2.0 wt.% of Pr^{3+}.

	CAS2:2.0Pr^{3+}				LSCAS2:2.0Pr^{3+}			
	Standard		Flórez *et al.*		Standard		Flórez *et al.*	
Transition	A	β	A	β	A	β	A	β
$^3P_0 \rightarrow$								
$^3H_4$	88851	0.610	81438	0.098	110920	0.669	103230	0.117
$^3H_5$	0	0	0	0	0	0	0	0
$^3H_6$	10785	0.074	7111	0.009	8232	0.050	4475	0.005
$^3F_2$	26144	0.180	37286	0.045	22148	0.134	33752	0.038
$^3F_3$	0	0	684601	0.826	0	0	718186	0.814
$^3F_4$	15868	0.109	14544	0.018	19661	0.119	18299	0.021
$^1G_4$	3905	0.027	3580	0.004	4917	0.030	4577	0.005
	$\tau = 6.87\ \mu s$		$\tau = 1.21\ \mu s$		$\tau = 6.03\ \mu s$		$\tau = 1.13\ \mu s$	
	$\tau_{exp} = (2.1 \pm 0.2)\ \mu s$				$\tau_{exp} = (3.4 \pm 0.1)\ \mu s$			
$^1D_2 \rightarrow$								
$^3H_4$	10873	0.654	10759	0.046	12688	0.7	12571	0.053
$^3H_5$	82	0.005	5516	0.023	97	0.005	5590	0.024
$^3F_2$	2390	0.144	9507	0.04	2627	0.145	10096	0.042
$^3F_4$	2570	0.155	156820	0.666	2081	0.115	156234	0.657
$^1G_4$	697	0.042	52918	0.225	627	0.035	53210	0.224
	$\tau = 60.19\ \mu s$		$\tau = 4.25\ \mu s$		$\tau = 55.18\ \mu s$		$\tau = 6.87\ \mu s$	
	$\tau_{exp} = (14.1 \pm 0.2)\ \mu s$				$\tau_{exp} = (16.5 \pm 1)\ \mu s$			

efficiency. With this consideration, the results obtained with the theory of Flórez *et al.* presented values which are higher than the physically expected.

Tables 4.4 and 4.5 shows the J–O intensity parameters follow the trend $\Omega_4 > \Omega_6 > \Omega_2$ for all Pr^{3+} concentration, for both glass hosts. Generally speaking, Ω_2 parameter is correlated to the asymmetry and degree of covalency of the surroundings of the ion, which means the higher is the value of Ω_2 parameter, more asymmetric is the glass and the more covalent is the ligand field at the ion site [9, 39, 64]. The glasses studied in this work presented higher value of Ω_2 than aluminosilicate [2], borate [7, 9], and phosphate [11] glasses. This demonstrate the highly asymmetrical and covalent environment of this glasses. The Ω_6 in inversely proportional to the degree of covalency between the bond of oxygen and Pr^{3+}. Ω_4 and Ω_6 parameters are related to the degree of rigidity of the host [65].

Additionally, from Tables 4.8, 4.9 and 4.10 the transitions $^3P_0 \rightarrow {}^3H_4$ and $^1D_2 \rightarrow {}^3H_4$ presented a branching ratio greater than 60% for both glass hosts, reaching more than 80% for the $^1D_2 \rightarrow {}^3H_4$ transition of the LSCAS:1.0Pr^{3+}. In addition with the reasonably good emission quantum efficiencies of these levels, specially the $^1D_2 \rightarrow {}^3H_4$ transition of the LSCAS host, suggest its use as potential laser emission transitions [66].

Chapter 5

Conclusions and prospects

In this work, results for the absorption spectra showed the electronic transitions of Pr^{3+} in the 400–2500 nm range. The weaker transitions such as $^3H_4 \rightarrow {}^1G_4$, $^3H_6$ could only be clearly distinguished at the highest concentration of 2.0 wt.% of Pr^{3+}. In the luminescence characterization, we have observed the superposition of two bands relative to the $^3P_0 \rightarrow {}^3H_6$ and $^1D_2 \rightarrow {}^3H_4$ transitions. This idea was corroborated by luminescence decay measurements. We also have noticed an unusual variation on the peak intensity with concentration for $^3P_0 \rightarrow {}^3F_2$ and $^3P_0 \rightarrow {}^3F_4$ transitions, suggesting they are hypersensitive, even though the latter does not entirely obey the classic selection rules for the hypersensitive transitions. Luminescence decay measurements showed curves with strong non-exponential behavior caused by non-radiative transitions such as cross-relaxations channels. The decrease in lifetime constants with dopant concentration indicates concentration quenching. Additionally, we report the energy upconversion on Pr^{3+}–doped CAS and LSCAS hosts. The VIS–to–UVC upconversion, present only in the CAS host, could be potentially used in optical devices for disinfection in medical/biological facilities or even as a mean to purify water in remote regions using the blue light of the sun as the upconversion activator.

The Judd-Ofelt theory was applied in the Pr^{3+}-doped CAS and LSCAS glasses using the standard and two modified approaches. Results using the Kornienko *et al.* modified theory had two outputs: (i) when the value of parameter $\mathcal{A}$ was fixed to 10^{-5} cm, results were inferior than standard theory: the deviation δ_{rms} value was up to three times greater than standard theory. (ii) When the parameter $\mathcal{A}$ is let to vary, better results were achieved with $\mathcal{A} \sim 10^{-7}$ cm: the deviation δ_{rms} was about the same as standard theory. However, such magnitude corresponds to an energy of the 4f5d level of about 5×10^6 cm^{-1}, which is not right concerning Pr^{3+}. Using the modified theory of Flórez *et al.*, there were several sets with all positive intensity parameters. The one with smallest deviation was the Ω_k with $k = 2, 3, 4, 6$, presenting δ_{rms} about two times smaller than the standard theory, for both hosts. Spectroscopic properties were derived using the standard theory and the modified theory of Flórez *et al.*. Compared to the experimental data, the emission transition probabilities showed a better agreement with the standard theory. Same pattern is seen concerning the radiative lifetime. Although the root mean square deviation was used as a relative parameter of the quality of results, additional indicators must be taken into account, such as the agreement between experimental and derived spectroscopic quantities. In that sense, standard theory gives more realistic results, even though its known issues with the theory for Pr^{3+}, at least to the hosts studied in this work. Overall, some real improvement can be seen with the modified theories developed so far, however, results can be also quite inconsistent as demonstrated in this work, indicating there are some aspects in theory of the 4f-4f transitions that are not completely understood yet. For this reason, additional investigations are necessary. Finally, by the standard theory, the branching ratio was found to be over 60% for the $^3P_0 \rightarrow {}^3H_4$ and $^1D_2 \rightarrow {}^3H_4$ transitions, for both hosts, indicating potential candidates for solid-state laser devices.

Prospects

During this work, it was not possible to confirm whether the mechanism responsible for the UC in the glass hosts is ETU or ESA. For this reason, additional investigations, for instance, the measurement of lifetime decay of the 4f5d level by direct excitation (> 250 nm) could help to elucidate the true process behind the UC mechanism.

In this work, we could also see a substantial difference between the peak position and intensity of the UC emission band: ~ 270 nm for CAS host and ~ 300 nm for LSCAS host with the intensity of the UC in the CAS around 20 times greater than in LSCAS. This differences suggest an additional investigation could be done concerning the compositional dependence of the UC. Eventually, an optimal composition with most intense emission could be found, as well as a composition with the UC band displaced more to the UVC range, resulting in an optimal disinfection potential. A compositional study could also be done in order to investigate the behavior of the hypersensitive transitions.

Finally, as shown in this work, even though some improvement is achieved with the different modified Judd-Ofelt theories, they do not represent a definite theory whatsoever, just as the standard Judd-Ofelt theory is not. A refined approach for describing the intensities of the 4f-4f transitions of the rare-earth elements could also be proposed.

Appendix A

Judd-Ofelt calculation algorithm

For the calculations of the Judd-Ofelt parameters and the spectroscopic properties the *Wolfram Mathematica 7.1* software was employed. Figure A.1 shows the main algorithm.

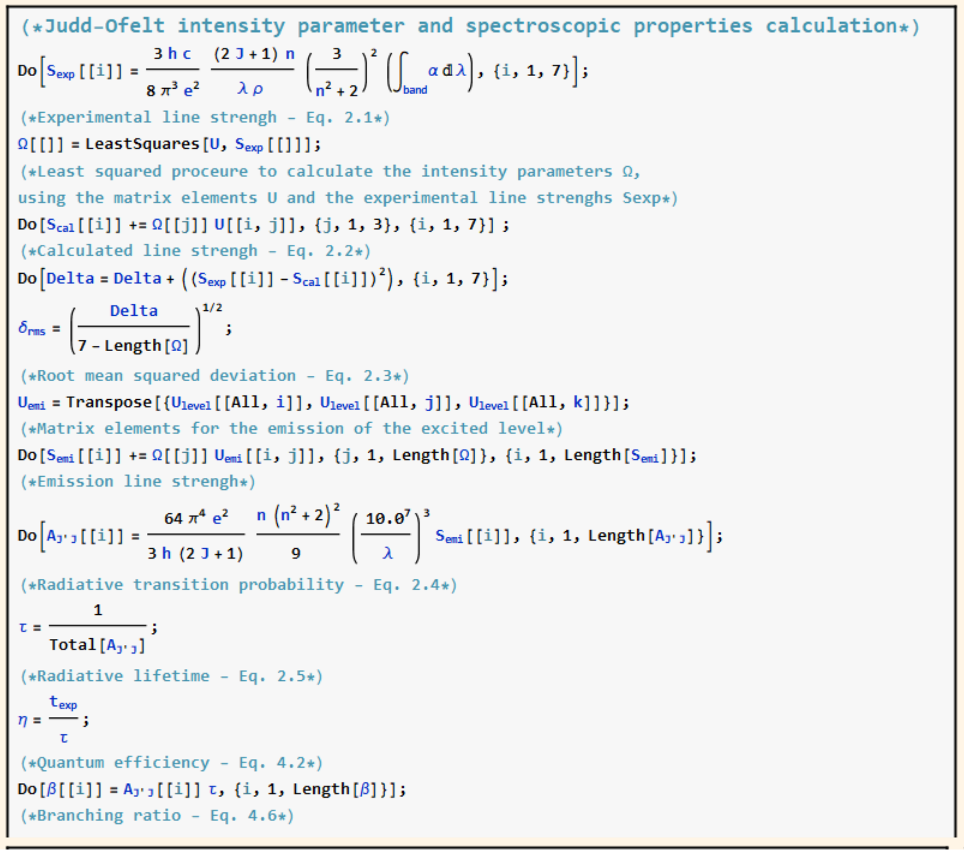

```
(*Judd-Ofelt intensity parameter and spectroscopic properties calculation*)
Do[Sexp[[i]] = (3 h c)/(8 π^3 e^2) ((2 J + 1) n)/(λ ρ) (3/(n^2 + 2))^2 (∫band α ⅆλ), {i, 1, 7}];
(*Experimental line strengh - Eq. 2.1*)
Ω[[]] = LeastSquares[U, Sexp[[]]];
(*Least squared proceure to calculate the intensity parameters Ω,
using the matrix elements U and the experimental line strenghs Sexp*)
Do[Scal[[i]] += Ω[[j]] U[[i, j]], {j, 1, 3}, {i, 1, 7}] ;
(*Calculated line strengh - Eq. 2.2*)
Do[Delta = Delta + ((Sexp[[i]] - Scal[[i]])^2), {i, 1, 7}];
δrms = (Delta/(7 - Length[Ω]))^(1/2) ;
(*Root mean squared deviation - Eq. 2.3*)
Uemi = Transpose[{Ulevel[[All, i]], Ulevel[[All, j]], Ulevel[[All, k]]}];
(*Matrix elements for the emission of the excited level*)
Do[Semi[[i]] += Ω[[j]] Uemi[[i, j]], {j, 1, Length[Ω]}, {i, 1, Length[Semi]}];
(*Emission line strengh*)
Do[AJ'J[[i]] = (64 π^4 e^2)/(3 h (2 J + 1)) (n (n^2 + 2)^2)/9 (10.0^7/λ)^3 Semi[[i]], {i, 1, Length[AJ'J]}];
(*Radiative transition probability - Eq. 2.4*)
τ = 1/Total[AJ'J];
(*Radiative lifetime - Eq. 2.5*)
η = texp/τ;
(*Quantum efficiency - Eq. 4.2*)
Do[β[[i]] = AJ'J[[i]] τ, {i, 1, Length[β]}];
(*Branching ratio - Eq. 4.6*)
```

Figure A.1: Main algorithm for the Judd-Ofelt calculations.

Appendix B

Published papers

A. Gonçalves, V.S. Zanuto, **G.A.S. Flizikowski**, A.N. Medina, F.L. Hegeto, A. Somer, J.L. Gomes Jr., J.V. Gunha, G.K. Cruz, C. Jacinto, N.G.C. Astrath, A. Novatski, “Luminescence and upconversion processes in Er^{3+}-doped tellurite glasses”, J. Lumin. **201**, (2018) 110-114.

G.A.S. Flizikowski, V.S. Zanuto, A. Novatski, L.A.O. Nunes, L.C. Malacarne, M.L. Baesso, N.G.C. Astrath, “Upconversion luminescence and hypersensitive transitions of Pr^{3+}–doped calcium aluminosilicate glasses”, J. Lumin. **202**, (2018) 27-31.

Journal of Luminescence 201 (2018) 110–114

Contents lists available at ScienceDirect

Journal of Luminescence

journal homepage: www.elsevier.com/locate/jlumin

Luminescence and upconversion processes in Er^{3+}-doped tellurite glasses

A. Gonçalves[a,b], V.S. Zanuto[b], G.A.S. Flizikowski[b], A.N. Medina[b], F.L. Hegeto[b], A. Somer[a], J.L. Gomes Jr.[a], J.V. Gunha[a], G.K. Cruz[a], C. Jacinto[c], N.G.C. Astrath[b], A. Novatski[a,*]

[a] *Departamento de Física, Universidade Estadual de Ponta Grossa, Ponta Grossa, PR 84030-900, Brazil*
[b] *Departamento de Física, Universidade Estadual de Maringá, Maringá, PR 87020-900, Brazil*
[c] *Instituto de Física, Universidade Federal de Alagoas, Maceió, AL 57072-900, Brazil*

ARTICLE INFO

Keywords:
Tellurite glasses
Erbium-doped
Luminescence
Upconversion

ABSTRACT

This work presents a spectroscopic investigation of tellurite glasses with the composition $65TeO_2$-$15Li_2O$-$20ZnO$ doped with different concentrations of Er_2O_3. Optical absorption and emission spectroscopy were performed at room temperature to determine emission properties of Er^{3+} in the visible and near-infrared regions. The samples presented intense green emission due to the $^2H_{11/2} \rightarrow {}^4I_{15/2}$ and $^4S_{3/2} \rightarrow {}^4I_{15/2}$ transitions. Emission intensities at 992 and 1550 nm exhibit a relative increase with increasing doping concentration. Luminescence decay curves for the $^4S_{3/2} \rightarrow {}^4I_{15/2}$ transition follows a non-exponential behavior, while the $^4I_{11/2} \rightarrow {}^4I_{15/2}$ and $^4I_{13/2} \rightarrow {}^4I_{15/2}$ transitions presented simple exponential behavior with high lifetime values. Under 975 nm excitation, upconversion luminescences in the green and red regions are observed, with a relative increase for red emission as function of doping concentration. The possible mechanisms considering multi-phonon relaxation, energy transfer and cross-relaxation processes were discussed for green and red emissions under excitations at 488 and 975 nm. The square dependence of green emission on the excitation power indicates two photons contribution to the upconversion emission. The full width at half-maximum values of emission at 1550 nm increased with increasing Er^{3+} concentration, showing the potential of the studied material as infrared amplifier.

1. Introduction

Rare-earth doped materials are widely used in photonics with vast applicability in optical amplifiers and solid state lasers, which require high emission quantum yields [1–5]. To produce functional devices, the development of these materials must have improved quantum yield at selected wavelengths. The property that directly affects the quantum yield is the energy loss due to nonradiative interactions [6]. TeO_2-based glasses, for instance, are attractive for such applications due the low vibrational frequencies (800 cm^{-1}), in addition to the high refractive index (2.1–2.3), good thermal and chemical stability, wide spectral transparency range (0.3–5 μm), and low melting point (~ 700 °C) [7–9].

Differently from other network formers such as SiO_2, B_2O_3 and P_2O_5 [10], TeO_2-based glasses require the addition of alkali oxides (Li_2O, Na_2O, K_2O) in their composition to facilitate vitrification [11]. The addition of Li_2O into TeO_2 glass leads to a decrease in the glass transition, which increases the thermal stability and changes the optical properties of the system [7,12]. One way to track-back these optical properties is to add transition metal oxides such as ZnO, Nb_2O_5 and Ag_2O [13–15] in the glass composition. Oxides can change their role as network modifier/former depending upon their concentration. As network modifier, ZnO oxide decreases the network connectivity, which can be a drawback for optical applications [13]. Otherwise, as network former, ZnO can promote the formation of $Zn_2Te_3O_8$ units increasing the network connectivity leading to systems with promising properties to act as hosts for optically active ions [14,16].

In this sense, Er^{3+}- doped zinc-tellurite glasses are interesting materials to achieve favorable emissions at blue, green, and red colors and at 1.5 μm [17–20]. Emissions in visible range can be achieved by upconversion processes using near-infrared (NIR) radiation [21] as excitation due to intermediate levels with long lifetimes ($^4I_{11/2}$ and $^4I_{13/2}$). Besides, these emissions drew a lot of attention due to their applications in modern lighting devices and optical displays [22–25].

Since the current demand for transmission capacity of wavelength division multiplexed telecommunication systems from *C* band (1530–1565 nm) to *L* band (1570–1610 nm) [19] has increased, the bandwidth of silica-based erbium-doped fiber amplifier (EDFA) (35 nm) has become insufficient [19]. If compared with silica glasses, Er^{3+}-doped tellurite glass presents broader emission (76 nm) and a larger stimulated emission cross-section [26,4], which are desirable properties for EDFA applications [27,28]. As the emission at 1.5 μm is strongly influenced by the host composition, it is important to investigate other

---

[*] Corresponding author.
E-mail addresses: ngcastrath@uem.br (N.G.C. Astrath), anovatski2@gmail.com (A. Novatski).

https://doi.org/10.1016/j.jlumin.2018.04.031
Received 30 January 2018; Received in revised form 13 April 2018; Accepted 13 April 2018

Journal of Luminescence 202 (2018) 27–31

Contents lists available at ScienceDirect

Journal of Luminescence

journal homepage: www.elsevier.com/locate/jlumin

Upconversion luminescence and hypersensitive transitions of Pr^{3+}–doped calcium aluminosilicate glasses

G.A.S. Flizikowski[a], V.S. Zanuto[a], A. Novatski[b], L.A.O. Nunes[c], L.C. Malacarne[a], M.L. Baesso[a], N.G.C. Astrath[a,*]

[a] *Departamento de Física, Universidade Estadual de Maringá, Maringá, PR 87020-900, Brazil*
[b] *Departamento de Física, Universidade Estadual de Ponta Grossa, Ponta Grossa, PR 84030-900, Brazil*
[c] *Instituto de Física de São Carlos, Universidade de São Paulo, São Carlos, SP 13560-970, Brazil*

ARTICLE INFO

Keywords:
Upconversion
Praseodymium
Hypersensitive
Aluminosilicate
Non-exponential decay

ABSTRACT

We present a detailed spectroscopic study of photoluminescence in calcium aluminosilicate glasses doped with different concentrations of Pr^{3+} (0.2, 0.5, 1.0 and 2.0 wt%). Optical transitions for the levels $^3H_4 \rightarrow {}^3P_{0,1,2}$; $^1I_6$; $^1D_2$; $^1G_4$; $^3F_{2,3,4}$ and $^3H_6$ have been observed using UV–Vis–NIR spectroscopy at room temperature. Emissions from levels $^3P_0$ and $^1D_2$ were detected and curves deviate from exponential behavior. Upconversion to UV was also observed when the samples were excited in the ^3P_j level, populating 4f5d upper level — via energy transfer upconversion and/or excited state absorption — which decays emitting UV light. In addition, the unusual variation of the peak intensities of transitions $^3P_0 \rightarrow {}^3F_2$ and $^3P_0 \rightarrow {}^3F_4$ suggests they are hypersensitive, although the $^3P_0 \rightarrow {}^3F_4$ electronic transition does not entirely obey all the classic selection rules.

1. Introduction

Calcium aluminosilicate glasses (CAS) have been extensively studied considering a number of applications for presenting appropriate physical properties such as high thermal conductivity, good mechanical strength and elevated transition temperature, besides transparency extending up to about 5 µm [1]. Several investigations have reported the effects of the composition of the glass on the physical properties [2,3], as well as spectroscopic features when CAS is doped with rare-earth ions. As rare-earth host, CAS glasses are potential candidates for application in optical devices such as tunable white light system [4,5] and solid state lasers [6,3,7].

Among rare-earth ions, trivalent praseodymium ion (Pr^{3+}) has been widely used for doping optical materials due to a broad infrared emission, which makes it interesting for telecommunication applications. Besides the infrared emission, Pr^{3+}–doped glasses exhibit a large visible emission spectrum, which comprises blue, green and orange-red emissions, depending on the host matrices [8]. As red emitting devices, these materials present great potential for applications in medical therapies due to the optical skin transmittance in this spectral range [9]. Alongside the variety of possible emissions, Pr^{3+} ions can also emit in the UV range when excited in the 4f5d level directly or via upconversion mechanisms.

Upconversion processes have been extensively studied for applications such as converting low-energy laser radiation into high-energy radiation by exchanging two or more low energy photons to one higher energy photon. This process has increased the response of solar cells in particular wavelengths [10–14] and, recently, studies showed the possibility to diagnose the Ebola virus using upconverting nanoparticles [15]. For Pr^{3+} ions, upconversion to UV has been studied, for instance, in ceramics [16] and crystals [17–19] and its origin could be due to energy transfer upconversion and/or simultaneous absorption of photons.

Despite the shielding of the 4–4f transitions that makes rare-earth elements unique, some transitions are very sensitives to the dopant environment, causing unusual alteration in the emission intensity — known as hypersensitive transitions. Reports showed hypersensitive transitions are affected by the dopant coordination, site symmetry, and ligand covalency [20,21]. These transitions, specifically, can be used in optical fiber amplifiers and lasers [20].

This work reports a spectroscopic study of Pr^{3+}–doped CAS glasses. The optical absorption spectra were obtained for the UV–Vis–NIR range and the photoluminescence spectra for the UV–Vis range. Luminescence decay measurements were also carried out to understand the energy processes involving Pr^{3+} ions in this particular glass matrix.

---

[*] Corresponding author.
E-mail address: ngcastrath@uem.br (N.G.C. Astrath).

https://doi.org/10.1016/j.jlumin.2018.05.009
Received 1 December 2017; Received in revised form 19 March 2018; Accepted 4 May 2018

Appendix C

Elsevier's permission to use published papers in a dissertation/thesis

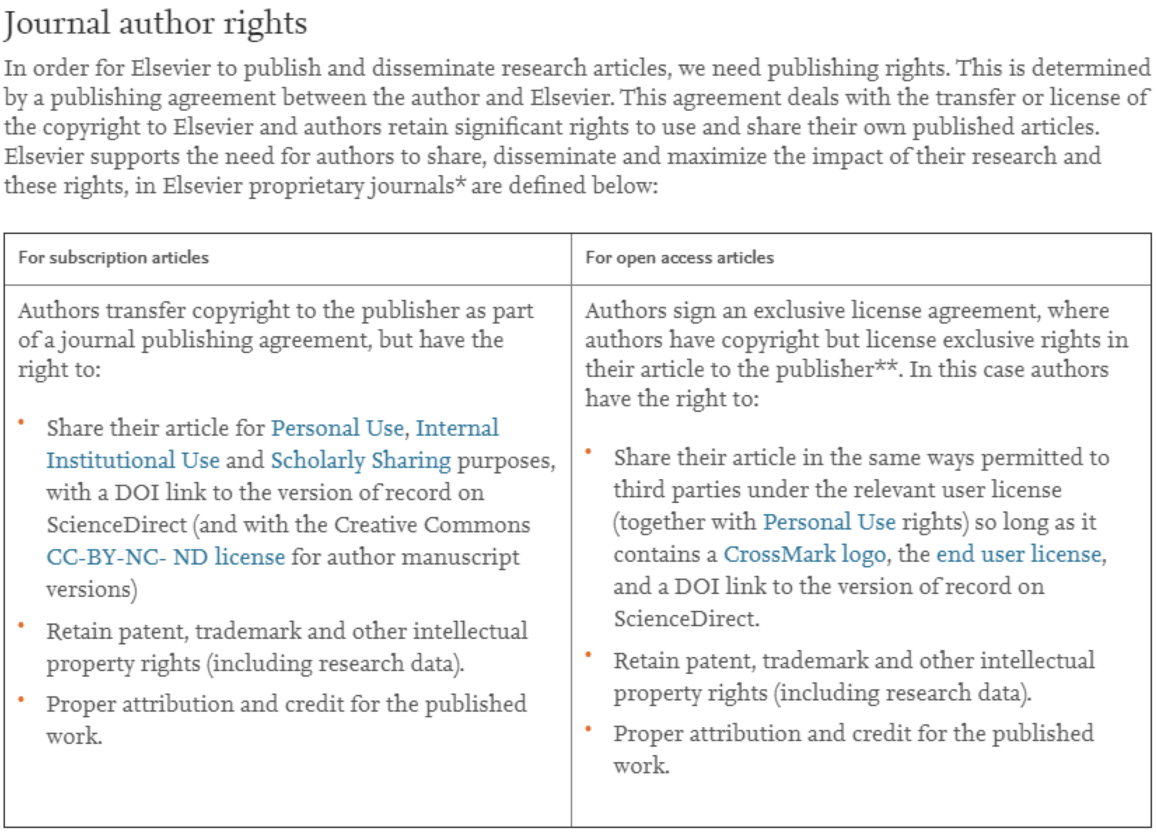

Journal author rights

In order for Elsevier to publish and disseminate research articles, we need publishing rights. This is determined by a publishing agreement between the author and Elsevier. This agreement deals with the transfer or license of the copyright to Elsevier and authors retain significant rights to use and share their own published articles. Elsevier supports the need for authors to share, disseminate and maximize the impact of their research and these rights, in Elsevier proprietary journals* are defined below:

For subscription articles	For open access articles
Authors transfer copyright to the publisher as part of a journal publishing agreement, but have the right to: • Share their article for Personal Use, Internal Institutional Use and Scholarly Sharing purposes, with a DOI link to the version of record on ScienceDirect (and with the Creative Commons CC-BY-NC- ND license for author manuscript versions) • Retain patent, trademark and other intellectual property rights (including research data). • Proper attribution and credit for the published work.	Authors sign an exclusive license agreement, where authors have copyright but license exclusive rights in their article to the publisher**. In this case authors have the right to: • Share their article in the same ways permitted to third parties under the relevant user license (together with Personal Use rights) so long as it contains a CrossMark logo, the end user license, and a DOI link to the version of record on ScienceDirect. • Retain patent, trademark and other intellectual property rights (including research data). • Proper attribution and credit for the published work.

Figure C.1: Extracted from Elsevier's website in the section "copyright" at `www.elsevier.com/about/policies/copyright`

Can I include/use my article in my thesis/dissertation? –

Yes. Authors can include their articles in full or in part in a thesis or dissertation for non-commercial purposes.

Figure C.2: Extracted from Elsevier's website in the section "permissions" at `www.elsevier.com/about/policies/copyright/permissions`

Bibliography

[1] S.-Z. Ma, W.-L. Feng, R. Chen, and Z.-Q. Peng, “KSr4(BO3)3:Pr3+: A new red-emitting phosphor for blue-pumped white light-emitting diodes,” *J. Alloys Compd.*, vol. 700, pp. 49–53, 2017.

[2] P. V. Lakshmi, T. S. Rao, K. Neeraja, D. V. K. Reddy, N. Veeraiah, and M. R. Reddy, “Fluorescence spectroscopic studies of Mn 2+ ions in SrO – Al2O3 – B2O3 – SiO2 glass system,” *J. Lumin.*, vol. 190, pp. 379–385, 2017.

[3] J. A. Medeiros Neto, D. W. Hewak, and H. Tate, “Application of a modified Judd-Ofelt theory to praseodymium-doped fluoride glasses,” *J. Non. Cryst. Solids*, vol. 183, no. 1-2, pp. 201–207, 1995.

[4] B. E. Bowlby and B. Di Bartolo, “Applications of the Judd-Ofelt theory to the praseodymium ion in laser solids,” *J. Lumin.*, vol. 100, no. 1-4, pp. 131–139, 2002.

[5] D. Manzani, D. Pabœuf, S. J. L. Ribeiro, P. Goldner, and F. Bretenaker, “Orange emission in Pr3+-doped fluoroindate glasses,” *Opt. Mater. (Amst).*, vol. 35, no. 3, pp. 383–386, 2013.

[6] P. Babu and C. K. Jayasankar, “Spectroscopy of Pr3+ ions in lithium borate and lithium glasses,” *Phys. B*, vol. 301, pp. 326–340, 2001.

[7] P. Srivastava, S. B. Rai, and D. K. Rai, “Effect of lead oxide on optical properties of Pr3+ doped some borate based glasses,” *J. Alloys Compd.*, vol. 368, no. 1-2, pp. 1–7, 2004.

[8] M. Rozanski, K. Wisniewski, J. Szatkowski, C. Koepke, and M. SRoda, “Effect of thermal treatment on excited state spectroscopy of oxyfluoride borosilicate glass activated by Pr3+ ions,” *Opt. Mater. (Amst).*, vol. 31, no. 3, pp. 548–553, 2009.

[9] I. Pal, A. Agarwal, S. Sanghi, and M. P. Aggarwal, “Structural, absorption and fluorescence spectral analysis of Pr 3+ ions doped zinc bismuth borate glasses,” *J. Alloys Compd.*, vol. 509, no. 28, pp. 7625–7631, 2011.

[10] V. Naresh and B. S. Ham, “Influence of multiphonon and cross relaxations on 3P0 and 1D2 emission levels of Pr3+ doped borosilicate glasses for broad band signal amplification,” *J. Alloys Compd.*, vol. 664, pp. 321–330, 2016.

[11] G. Ajithkumar, P. K. Gupta, G. Jose, and N. V. Unnikrishnan, “Judd-Ofelt intensity parameters and laser analysis of Pr3+doped phosphate glasses sensitized by Mn2+ions,” *J. Non. Cryst. Solids*, vol. 275, no. 1, pp. 93–106, 2000.

[12] L. R. Moorthy, A. Radhapathy, M. Jayasimhadri, T. S. Rao, D. V. R. Murthy, and S. A. Saleem, “Modified Judd-Ofelt analysis of Pr3+ ions in mixed alkali chloroborophosphate glasses,” *Phys. B*, vol. 352, no. 1-4, pp. 210–219, 2004.

[13] M. P. Belançon, J. D. Marconi, M. F. Ando, and L. C. Barbosa, “Near-IR emission in Pr3+single doped and tunable near-IR emission in Pr3+/Yb3+ codoped tellurite tungstate glasses for broadband optical amplifiers,” *Opt. Mater. (Amst).*, vol. 36, no. 6, pp. 1020–1026, 2014.

[14] F. Zhang, Z. Bi, A. Huang, and Z. Xiao, “Luminescence and Judd-Ofelt analysis of the Pr3+ doped fluorotellurite glass,” *J. Lumin.*, vol. 160, no. 37, pp. 85–89, 2015.

[15] L. J. Borrero-González, L. A. O. Nunes, J. L. Carmo, F. B. G. Astrath, and M. L. Baesso, “Spectroscopic studies and downconversion luminescence in OH – free Pr3+-Yb3+ co-doped low-silica calcium aluminosilicate glasses,” *J. Lumin.*, vol. 145, pp. 615–619, 2014.

[16] A. Steimacher, N. G. C. Astrath, A. Novatski, F. Pedrochi, A. C. Bento, M. L. Baesso, and A. N. Medina, “Characterization of thermo-optical and mechanical properties of calcium aluminosilicate glasses,” *J. Non. Cryst. Solids*, vol. 352, no. 32-35, pp. 3613–3617, 2006.

[17] M. L. Baesso, A. C. Bento, A. A. Andrade, T. Catunda, J. A. Sampaio, and S. Gama, “Neodymium concentration dependence of thermo-optical properties in low silica calcium aluminate glasses,” *J. Non. Cryst. Solids*, vol. 219, pp. 165–169, 1997.

[18] A. Steimacher, M. J. Barboza, A. M. Farias, O. A. Sakai, J. H. Rohling, A. C. Bento, M. L. Baesso, A. N. Medina, and C. M. Lepienski, “Preparation of Nd2O3-doped calcium aluminosilicate glasses and thermo-optical and mechanical characterization,” *J. Non. Cryst. Solids*, vol. 354, no. 42-44, pp. 4749–4754, 2008.

[19] L. J. Borrero-González, I. A. A. Terra, L. A. O. Nunes, A. M. Farias, M. J. Barboza, J. H. Rohling, A. N. Medina, and M. L. Baesso, “The influence of SiO2 content on spectroscopic properties and laser emission efficiency of Yb3+-Er3+ co-doped calcium aluminosilicate glasses,” *Appl. Phys. B*, vol. 107, no. 2, pp. 415–420, 2012.

[20] S. M. Lima, L. H. C. Andrade, A. C. P. Rocha, J. R. Silva, A. M. Farias, A. N. Medina, M. L. Baesso, L. A. O. Nunes, Y. Guyot, and G. Boulon, “Eu2+-doped OH- free calcium aluminosilicate glass: A phosphor for smart lighting,” *J. Lumin.*, vol. 143, pp. 600–604, 2013.

[21] L. H. C. Andrade, S. M. Lima, A. Novatski, P. T. Udo, N. G. C. Astrath, A. N. Medina, A. C. Bento, M. L. Baesso, Y. Guyot, and G. Boulon, “Long fluorescence lifetime of Ti3+-doped low silica calcium aluminosilicate glass,” *Phys. Rev. Lett.*, vol. 100, no. 2, p. 027402, 2008.

[22] A. Steimacher, M. J. Barboza, F. Pedrochi, N. G. C. Astrath, J. H. Rohling, M. L. Baesso, and A. N. Medina, “Nd3+doped CAS glasses: A thermo-optical and spectroscopic investigation,” *Opt. Mater. (Amst).*, vol. 37, no. C, pp. 531–536, 2014.

[23] L. S. Costa, *Investigação da eficiência quântica de luminescência pela teoria de Judd-Ofelt: Aplicação aos vidros Aluminosilicato de Cálcio dopados com Érbio.* Dissertation, Universidade Estadual de Maringá, 2014.

[24] A. Jaworski, *Structure of Rare-Earth Aluminosilicate Glasses Probed by Solid-State NMR Spectroscopy and Quantum Chemical Calculations.* Doctoral dissertation in physical chemistry, Stockholm University, 2016.

[25] S. Fischer, J. C. Goldschmidt, P. Löper, G. H. Bauer, R. Brüggemann, K. Krämer, D. Biner, M. Hermle, and S. W. Glunz, “Enhancement of silicon solar cell efficiency by upconversion: Optical and electrical characterization,” *J. Appl. Phys.*, vol. 108, p. 044912, 2010.

[26] J. de Wild, J. K. Rath, A. Meijerink, W. G. J. H. M. van Sark, and R. E. I. Schropp, “Enhanced near-infrared response of a-Si:H solar cells with β-NaYF 4:Yb3 (18%), Er3 (2%) upconversion phosphors,” *Sol. Energy Mater. Sol. Cells*, vol. 94, no. 12, pp. 2395–2398, 2010.

[27] W. G. J. H. M. van Sark, J. de Wild, J. K. Rath, A. Meijerink, and R. E. I. Schropp, “Upconversion in solar cells,” *Nanoscale Res. Lett.*, vol. 8, no. 1, p. 81, 2013.

[28] Y. Shang, S. Hao, C. Yang, and G. Chen, “Enhancing Solar Cell Efficiency Using Photon Upconversion Materials,” *Nanomaterials*, vol. 5, no. 4, pp. 1782–1809, 2015.

[29] S. Asahi, H. Teranishi, K. Kusaki, T. Kaizu, and T. Kita, “Two-step photon up-conversion solar cells,” *Nat. Commun.*, vol. 8, p. 14962, 2017.

[30] M.-K. Tsang, W. Ye, G. Wang, J. Li, M. Yang, and J. Hao, “Ultrasensitive detection of Ebola virus oligonucleotide based on upconversion nanoprobe/nanoporous membrane system,” *ACS Nano*, vol. 10, no. 1, pp. 598–605, 2016.

[31] E. L. Cates, A. P. Wilkinson, and J.-H. Kim, “Visible-to-UVC upconversion efficiency and mechanisms of Lu7O6F9:Pr3+ and Y2SiO5:Pr3+ ceramics,” *J. Lumin.*, vol. 160, pp. 202–209, 2015.

[32] C. Hu, C. Sun, J. Li, Z. Li, H. Zhang, and Z. Jiang, “Visible-to-ultraviolet upconversion in Pr3+:Y2SiO5 crystals,” *Chem. Phys.*, vol. 325, pp. 563–566, 2006.

[33] H. Yang, Z. Dai, N. Zu, H. Zhang, and Z. Jiang, “Ultraviolet broad emission of Prˆ3+:Y_2SiO_5 crystal by 532 nm two-photon absorption,” *J. Opt. Soc. Am. B*, vol. 24, no. 5, pp. 1178–1180, 2007.

[34] X. Wang, J. Qiu, J. Song, J. Xu, Y. Liao, H. Sun, Y. Cheng, and Z. Xu, “Simultaneous three-photon absorption induced ultraviolet upconversion in Pr3+:Y2SiO5 crystal by femtosecond laser irradiation,” *Opt. Commun.*, vol. 281, no. 2, pp. 299–302, 2008.

[35] V. K. Tikhomirov, M. Naftaly, and A. Jha, “Effects of the site symmetry and host polarizability on the hypersensitive transition P-3(0)-> F-3(2) of Pr3+ in fluoride glasses,” *J. Appl. Phys.*, vol. 86, no. 1, pp. 351–354, 1999.

[36] V. K. Tikhomirov and S. A. Tikhomirova, “Hypersensitive transition 3 P 0 3 F 2 of Pr 3 related to the polarizability and structure of glass host,” *J. Non. Cryst. Solids*, vol. 274, pp. 50–54, 2000.

[37] B. R. Judd, “Optical absorption intensities of rare-earth ions,” *Phys. Rev.*, vol. 127, no. 3, pp. 750–761, 1962.

[38] G. S. Ofelt, “Intensities of crystal spectra of rare-earth ions,” *J. Chem. Phys.*, vol. 37, no. 1962, pp. 511–520, 1962.

[39] C. K. Jørgensen and R. Reisfeld, “Judd-Ofelt parameters and chemical bonding,” *J. Less-Common Met.*, vol. 93, no. 1, pp. 107–112, 1983.

[40] C. Jacinto, *Caracterização Termo-Óptica de Materias Lasers Usando a Técnica de Lente Térmica.* Thesis, Universidade de São Paulo, 2006.

[41] M. J. Weber, T. E. Varitimos, and B. H. Matsinger, “Optical intensities of rare-earth ions in yttrium orthoaluminate,” *Phys. Rev. B*, vol. 8, no. 1, pp. 47–53, 1973.

[42] M. P. Hehlen, M. G. Brik, and K. W. Krämer, “50th anniversary of the Judd-Ofelt theory: An experimentalist’s view of the formalism and its application,” *J. Lumin.*, vol. 136, pp. 221–239, 2013.

[43] R. Hakim, K. Damak, A. Toncelli, M. Fourati, and R. Maalej, “Growth, optical spectroscopy and Judd-Ofelt analysis of Pr-doped BaY 2F8 monocrystals,” *J. Lumin.*, vol. 143, pp. 233–240, 2013.

[44] A. A. Kornienko, A. A. Kaminskii, and E. B. Dunina, “Dependence of Line Strength of Electrical Dipole F-F Transitions on the Multiplet Energy of Pr-3+ Ion in Yalo3,” *Phys. status solidi B*, vol. 157, no. 1, p. 261, 1990.

[45] A. A. Kornienko, A. A. Kaminskii, and E. B. Dunina, “Dependence of Line Strength of Electrical Dipole F-F Transitions on the Multiplet Energy of Pr-3+ Ion in Yalo3,” *Phys. status solidi B*, vol. 157, no. 1, p. 267, 1990.

[46] A. Flórez, O. L. Malta, Y. Messaddeq, and M. A. Aegerter, “Judd–Ofelt analysis of Pr3+ ions in fluoroindate glasses: influence of odd third order intensity parameters,” *J. Non. Cryst. Solids*, vol. 213-214, pp. 315–320, 1997.

[47] A. Flórez, M. Flórez, Y. Messaddeq, M. A. Aegerter, and P. Porcher, “Application of standard and modifed Judd-Ofelt theories to thulium doped fuoroindate glass,” *J. Non. Cryst. Solids*, vol. 247, pp. 215–221, 1999.

[48] A. B. Spierings, M. Schneider, and R. Eggenberger, “Comparison of density measurement techniques for additive manufactured metallic parts,” *Rapid Prototyp. J.*, vol. 17, no. 5, pp. 380–386, 2011.

[49] S. Schutzmann, M. Casalboni, F. De Matteis, and P. Prosposito, “Refractive index measurements of thin films using both Brewster and m-line technique: A combined experimental setup,” *J. Non. Cryst. Solids*, vol. 351, no. 21-23, pp. 1814–1818, 2005.

[50] E. Grace, A. Butcher, J. Monroe, and J. A. Nikkel, “Index of refraction, Rayleigh scattering length, and Sellmeier coefficients in solid and liquid argon and xenon,” *Nucl. Instruments Methods Phys. Res. Sect. A Accel. Spectrometers, Detect. Assoc. Equip.*, vol. 867, no. June, pp. 204–208, 2017.

[51] H. Chen, R. Lian, M. Yin, L. Lou, W. Zhang, S. Xia, and J.-C. Krupa, “Luminescence concentration quenching of 1 D 2 state in YPO 4 : Pr 3 +,” *J. Phys. Condens. Matter*, vol. 13, pp. 1151–1158, 2001.

[52] S. H. Huang, X.-J. Wang, B.-J. Chen, D. Jia, and W. M. Yen, “Photon cascade emission and quantum efficiency of the 3P0 level in Pr3+-doped SrAl12O19 system,” *J. Lumin.*, vol. 102-103, no. SPEC, pp. 344–348, 2003.

[53] S. Babu, P. Rajput, and Y. C. Ratnakaram, “Compositional-dependent properties of Pr 3+ -doped multicomponent fluoro- phosphate glasses for visible applications: a photoluminescence study,” *J. Mater. Sci.*, vol. 51, no. 51, pp. 8037–8054, 2016.

[54] V. Vidyadharan, S. Gopi, M. P. Remya, V. Thomas, C. Joseph, N. V. Unnikrishnan, and P. R. Biju, “Judd-Ofelt analysis of Pr3+ ions in Sr1.5Ca0.5SiO4 and Sr0.5Ca0.5TiO3 host matrices,” *Opt. Mater. (Amst).*, vol. 51, pp. 62–69, 2016.

[55] I. E. Seferis, K. Fiaczyk, D. Spassky, E. Feldbach, I. Romet, M. Kirm, and E. Zych, “Synthesis and luminescence properties of BaHfO 3 : Pr ceramics,” *J. Lumin.*, vol. 189, pp. 148–152, 2017.

[56] C. P. Reddy, V. Naresh, and K. T. R. Reddy, “Optical and spectral analysis of Pr 3+ doped lithium zinc fluoro telluro phosphate glasses,” *Mater. Today Proc.*, vol. 3, no. 10, pp. 4058–4063, 2016.

[57] X. Li, C. Liang, S. Guo, Y. Xiao, and C. Chang, “Photoluminescence and afterglow behavior of Tb 3+ activated Li 2 SrSiO 4 phosphor,” *J. Lumin.*, vol. 188, no. November 2016, pp. 199–203, 2017.

[58] R. Chen, “Apparent stretched-exponential luminescence decay in crystalline solids,” *J. Lumin.*, vol. 102-103, no. SPEC, pp. 510–518, 2003.

[59] R. F. Muniz, D. de Ligny, S. Le Floch, C. Martinet, J. H. Rohling, A. N. Medina, M. Sandrini, L. H. C. Andrade, S. M. Lima, M. L. Baesso, and Y. Guyot, “On the induction of homogeneous bulk crystallization in Eu-doped calcium aluminosilicate glass by applying simultaneous high pressure and temperature,” *J. Appl. Phys.*, vol. 119, no. 24, p. 245901, 2016.

[60] X. Zhou, X. Zhao, C. S. K. Mak, L. Li, Q. Li, and P. A. Tanner, “Yellow to violet upconversion processes of Nd3+in neat Cs2NaNdCl6 elpasolite,” *Opt. Mater. (Amst).*, vol. 37, pp. 24–27, 2014.

[61] M. Pollnau, D. R. Gamelin, S. R. Lüthi, H. U. Güdel, and M. P. Hehlen, “Power dependence of upconversion luminescence in lanthanide and transition-metal-ion systems,” *Phys. Rev. B*, vol. 61, no. 5, pp. 3337–3346, 2000.

[62] T. Dai, M. S. Vrahas, C. K. Murray, and M. R. Hamblin, “Ultraviolet C irradiation: an alternative antimicrobial approach to localized infections?,” *Expert Rev. Anti Infect. Ther*, vol. 10, pp. 185–195, 2012.

[63] R. T. Génova, I. R. Martín, U. R. Rodríguez-Mendoza, F. Lahoz, A. D. Lozano-Gorrín, P. Núñez, J. González-Platas, and V. Lavín, "Optical intensities of Pr3+ions in transparent oxyfluoride glass and glass-ceramic. Applications of the standard and modified Judd-Ofelt theories," *J. Alloys Compd.*, vol. 380, no. 1-2 SPEC. ISS., pp. 167–172, 2004.

[64] M. El Okr, M. Farouk, M. El-Sherbiny, M. A. K. El-Fayoumi, and M. G. Brik, "Spectroscopic studies of the Pr3+-doped borovanadate glass," *J. Alloys Compd.*, vol. 490, no. 1-2, pp. 184–189, 2010.

[65] G. Lakshminarayana, J. Qiu, M. G. Brik, G. A. Kumar, and I. V. Kityk, "Spectral analysis of RE3+ (RE = Er, Nd, Pr and Ho):GeO 2-B2O3-ZnO-LiF glasses," *J. Phys. Condens. Matter*, vol. 20, no. 37, 2008.

[66] V. Ravi Kumar, N. Veeraiah, B. Appa Rao, and S. Bhuddudu, "Optical absorption and photoluminescence properties of Eu3+-doped ZnF2–PbO–TeO2 glasses," *J. Mater. Sci.*, vol. 33, no. 10, pp. 2659–2662, 1998.